A MYC/GCN2/eIF2α negative feedback loop limits protein synthesis to prevent MYC-dependent apoptosis in colorectal cancer

Stefanie Schmidt[1,2*], David Gay[3*], Friedrich Wilhelm Uthe[1,2*], Sarah Denk[1,2], Madelon Paauwe[3], Niels Matthes[1,2], Markus Elmar Diefenbacher[1], Sheila Bryson[3], Fiona Clare Warrander[3], Florian Erhard[4], Carsten Patrick Ade[1], Apoorva Baluapuri[1], Susanne Walz[5], Rene Jackstadt[3], Catriona Ford[3], Georgios Vlachogiannis[6], Nicola Valeri[6,7], Christoph Otto[2], Christina Schülein-Völk[1], Katja Maurus[8], Werner Schmitz[1], John Raymond Philip Knight[3], Elmar Wolf[1], Douglas Strathdee[3], Almut Schulze[1,8], Christoph-Thomas Germer[2,8], Andreas Rosenwald[8], Owen James Sansom[3,9], Martin Eilers[1,8§], and Armin Wiegering[1,2,8§]

[1)] Theodor Boveri Institute, Biocenter, University of Würzburg, Am Hubland, 97074 Würzburg, Germany

[2)] University Hospital Würzburg, Department of General, Visceral, Vascular and Pediatric Surgery, Würzburg, Germany

[3)] CRUK Beatson Institute, Garscube Estate, Switchback Road, Glasgow, G61 1BD, UK

[4)] Institute for Virology and Immunobiology, University of Würzburg, Versbacher Straße 7, 97078 Würzburg, Germany

[5)] Comprehensive Cancer Center Mainfranken, Core Unit Bioinformatics, Biocenter, University of Würzburg, Am Hubland, 97074 Würzburg, Germany

[6)] Division of Molecular Pathology, The Institute of Cancer Research, London, SW7 3RP, UK

[7)] Department of Medicine, The Royal Marsden NHS Trust, London, SW3 6JJ, UK

[8)] Comprehensive Cancer Center Mainfranken, University of Würzburg, Josef-Schneider-Str. 6, 97080 Würzburg, Germany

[9)] Institute of Cancer Sciences, University of Glasgow, Garscube Estate, Glasgow G61 1QH, UK

[*)] These authors contributed equally to the work.

[§)] Correspondence: wiegering_a@ukw.de; martin.eilers@biozentrum.uni-wuerzburg.de

Key words: colorectal cancer, APC, MYC, translation, eIF2B5, eIF2α

Word count abstract: 150

Word count: 3841

Total number of figures: 8

Abstract

Tumours depend on altered rates of protein synthesis for growth and survival, suggesting that mechanisms controlling mRNA translation may be exploitable for therapy. Here, we show that loss of APC, which occurs almost universally in colorectal tumours, strongly enhances the dependence on the translation initiation factor eIF2B5. Depletion of eIF2B5 induces an integrated stress response and enhances translation of MYC via an internal ribosomal entry site. This perturbs cellular amino acid and nucleotide pools and strains energy resources and causes MYC-dependent apoptosis. eIF2B5 limits MYC expression and prevents apoptosis in APC-deficient murine and patient-derived organoids and in APC-deficient murine intestinal epithelia *in vivo*. Conversely, the high MYC levels present in APC-deficient cells induce phosphorylation of eIF2α via the GCN2 and PKR kinases. Pharmacological inhibition of GCN2 phenocopies eIF2B5 depletion and has therapeutic efficacy in tumour organoids, demonstrating that a negative MYC/eIF2α feedback loop constitutes a targetable vulnerability of colorectal tumours.

Introduction

Overall rates of cellular protein synthesis are regulated by extracellular and cell-intrinsic signals. Specifically, recognition of the mRNA cap structure by eIF4F as well as binding and recycling of the ternary complex (TC) are tightly controlled steps during translation initiation [1, 2]. In response to stress signals, eIF2α, a component of the TC, is phosphorylated [3]. This enhances its affinity for eIF2B, which sequesters phosphorylated eIF2α into an inactive complex, and disrupts TC formation [4-6]. Reduction in TC levels inhibits global translation initiation, but enhances translation of stress-responsive mRNAs via the integrated stress response (ISR) [3].

Virtually all colorectal cancers (CRC) harbor activating mutations in the WNT signaling pathway. Most frequently, this is due to deletion or loss-of-function mutations of the *APC* tumour suppressor [7], leading to an upregulation of the transcription factor MYC [8]. Restoration of *Apc* or deletion of *Myc* ablates tumourigenesis in mouse models of CRC [9, 10]. MYC induces transcription of genes encoding proteins of the translation machinery [7], and enhances global protein synthesis [8, 11-13]. Interfering with translation initiation or the mTOR-eEF2K axis controlling translational elongation is tolerated by normal tissues but prevents CRC growth, arguing that CRC depends on enhanced protein synthesis [1, 11, 14-16].

Here, we searched for specific dependencies of APC-deficient CRCs. Starting from an unbiased genetic screen, we identified a negative feedback loop, in which deregulated MYC expression and global translation in APC-deficient cells induce phosphorylation of eIF2α, which limits protein synthesis. Using mouse tumour models as well as murine and patient-derived organoids, we validated this dependency. Disrupting this circuit either genetically or by small molecule inhibitors of eIF2α kinases has therapeutic efficacy in APC-deficient tumours.

Results

Restoration of APC expression suppresses translation and anchorage-independent growth

To identify genes that are essential in APC-deficient cells, we engineered SW480 cells, harbouring truncating mutations in both *APC* alleles, to express full-length APC in a doxycycline-inducible manner ($SW480^{TetOnAPC}$) (Fig. 1a and Extended Data 1a,b). We designate these cells APC-deficient (APC^{def}) in the absence and APC-restored (APC^{res}) in the presence of doxycycline. In APC^{res} cells, β-catenin protein levels and mRNA expression of *MYC*, *DKK1* and *AXIN2* were significantly downregulated (Fig. 1a,b,c and Extended Data 1b,c). Gene set enrichment analysis (GSEA) of RNA-sequencing data showed that induction of APC represses multiple WNT- and MYC-regulated genes (Fig. 1d), including genes encoding proteins involved in translation (Fig. 1d and Supplementary Table 1) [17-20]. Consistent with these data and previous observations, global protein synthesis was enhanced in APC^{def} cells (Fig. 1e) [11]. Restoration of APC did not affect cell growth in two-dimensional culture conditions and did not induce apoptosis (Fig. 1f, and Extended Data 1d). In contrast, the number and size of APC^{res} colonies growing in an anchorage-independent manner, a hallmark of oncogenic transformation [21], were markedly reduced (Fig. 1g,h,i) [22].

APC-deficient CRC cells depend on physiological eIF2B5 levels

To identify genes required for the growth of APC^{def}, but not of APC^{res} cells, we performed a dropout screen and infected $SW480^{TetOnAPC}$ cells with a lentiviral shRNA library targeting 5,000 potentially druggable genes encoding translation initiation and elongation factors as well as ribosomal proteins (Extended Data 1e,f). For each shRNA, relative enrichment or depletion after day 3 and day 15 of ethanol or doxycycline treatment was determined. Twenty-one shRNAs targeting luciferase, included as negative controls, were not selected against during growth of either APC^{def} or APC^{res} cells (Extended Data 1g). In contrast, four out of five shRNAs targeting *PSMB2*, encoding an essential component of the proteasome, led to growth disadvantage in both APC^{def} and APC^{res} cells (Extended Data 1h). Using a two-

fold difference in representation between APC^{def} and APC^{res} cells at day 15, but not at day 3, we filtered for potential hits (FDR < 0.05). From these, we recovered nine genes that were targeted by at least two shRNAs (Extended Data 1i and Supplementary Table 2). Among them were shRNAs targeting *BCL2L1,* which has previously been shown to be required for growth of cells with activating β-catenin mutations [23]. Notably, four out of five shRNAs targeting *EIF2B5* were depleted specifically in APC^{def} cells, and showed the greatest difference in shRNA representation (Fig. 2a). Consistent with recovery as a hit, eIF2B5 depletion by an shRNA, used in the screen, suppressed growth of APC^{def} cells, but had only minor effects on APC^{res} cells (Fig. 2b,c), despite similar knockdown efficiency (Fig. 2d,e). eIF2B5 depletion in APC^{def} cells, but not in APC^{res} cells, significantly increased the percentage of annexin V/PI-positive cells and the percentage of cells with a subG1 DNA content (Fig. 2f and Extended Data 2a).

Using a series of four shRNAs with different knockdown efficacy (Extended Data 2b), we established that differential apoptosis induction in APC^{def} and APC^{res} cells correlated with the degree of eIF2B5 depletion (Extended Data 2c). Strong knockdown elicited by sh*EIF2B5* #1 potently induced apoptosis in APC^{def}, but also to some degree in APC^{res} cells. Moderate knockdown by sh*EIF2B5* #3 induced apoptosis in APC^{def}, but had no effect on APC^{res} cells. Weak knockdown (sh*EIF2B5* #2, #4) induced little or no apoptosis in APC^{def} and APC^{res} cells. To validate that apoptosis is an on-target effect, we overexpressed an shRNA-resistant HA-tagged eIF2B5 (eIF2B5mut-HA). Neither sh*EIF2B5* #1 nor #3 depleted HA-tagged exogenous eIF2B5, although they are functional since they reduced expression of endogenous eIF2B5 (Extended Data 2d,e). Accordingly, we observed no apoptosis in cells expressing eIF2B5mut-HA (Extended Data 2f). Finally, eIF2B5 depletion strongly suppressed growth of APC-deficient HT29 cells, but had a much weaker effect in APC-proficient HCT116 cells (Fig. 2g,h and Extended Data 2g).

Notably, APC^{def} and APC^{res} cells express comparable eIF2B5 protein levels despite increased *EIF2B5* mRNA levels in APC^{def} relative to APC^{res} cells (Fig. 2d,e). Datasets from human CRCs show a moderate increase in *EIF2B5* mRNA in CRC relative to normal tissue (Extended Data 2h). Histopathologic staining of human CRC samples revealed an enhanced eIF2B5 expression in tumours relative to mucosa (Fig. 2i). We concluded that physiological levels of eIF2B5 are required to suppress apoptosis in APC-deficient cells.

eIF2B5 controls translation initiation and limits global protein synthesis

eIF2B5 is the catalytic subunit of the decameric eIF2B complex [4, 24, 25], which is the guanine nucleotide exchange factor (GEF) for eIF2 that replaces GDP by GTP and enables binding of initiator methionyl transfer RNA (Met-tRNAi) to eIF2 (TC formation) [24, 26]. Accordingly, eIF2B5 depletion caused a relative increase in free 40S and 60S ribosomal subunits and a decrease in polysomal fractions (Fig. 3a and Extended Data 3a). To pinpoint the effect on translation initiation, we blocked the first translation elongation step by addition of harringtonine [27]. This led to an expected increase in 40S, 60S, and 80S monosomes and showed that eIF2B5 depletion strongly reduced the amount of 80S monosomes consistent with its effect on TC formation (Fig. 3a). Surprisingly, eIF2B5 knockdown elicited an increase in overall protein synthesis in both APC^{def} and APC^{res} cells (Fig. 3b). This increase correlated with the degree of eIF2B5 knockdown (Extended Data 2b and 3b). In CRC cells, inhibition of initiation can be compensated by an increase in translation elongation driven via inhibition of eEF2K by S6K1 [11]. Accordingly, depletion of eIF2B5 strongly activated S6K1 in APC^{def} cells (Extended Data 3c).

Consistent with previous findings, eIF2α and its phosphorylated form are upregulated in tumour tissue [28] (Fig. 3c). In addition, eIF2B binds p-eIF2α with high affinity and antagonizes dephosphorylation and activation of eIF2α by PP1 [29]. Depletion of eIF2B5 led to dephosphorylation of eIF2α at S51, readily detectable in APC^{def} cells, while the effect in APC^{res} cells was more variable (Fig. 3d and Extended Data 3d). To determine whether

eIF2B5 limits PP1 binding to eIF2α, we immunoprecipitated eIF2α. Depletion of eIF2B5 strongly enhanced association of PP1 with eIF2α in APC^{def}, but much less so in APC^{res} cells (Fig. 3e). This mechanism is expected to reduce the sensitivity of translation initiation to inhibition by stress-related kinases.

Depletion of eIF2B5 causes MYC-driven apoptosis

To understand why eIF2B5 depletion causes apoptosis specifically of APC^{def} cells, we performed ribosome profiling of APC^{def} and APC^{res} cells to investigate a potential shift in the spectrum of translated mRNAs [30, 31]. We did not observe any differences in global ribosome association of mRNAs between eIF2B5-depleted APC^{def} and APC^{res} cells (Extended Data 3e and Supplementary Table 3). However, gene ontology analysis of ribosome-associated mRNAs revealed an enrichment of mRNAs associated with stress response and apoptotic signaling pathways upon eIF2B5 knockdown in APC^{def}, but less in APC^{res} cells (Extended Data 3f). This is consistent with observations that a reduction in TC formation induces an ISR resulting in a bypass of upstream open reading frames (uORFs) present in stress-responsive mRNAs such as that of the transcription factor ATF4 [2]. Indeed, inactivating mutations in eIF2B subunits in yeast lead to the induction of the ISR [32]. Accordingly, eIF2B5 knockdown induced ATF4 protein expression as well as enrichment of a consensus ATF4 target gene signature including *DDIT3*, *ATF3* and *ATF6*, in APC^{def} cells and this response correlates with the degree of eIF2B5 knockdown (Fig. 3f,g, Extended Data 3g and Supplementary Table 4).

Enhanced translation and defects in protein folding in the endoplasmic reticulum can activate two other stress signaling pathways, mediated by IRE1α and ATF6, as part of the unfolded protein response (UPR) [33]. Notably, while APC loss activated both the ISR and IRE1α as well as ATF6, evidenced by expression of UPR-associated genes (spliced *XBP1*, *GRP78* and unspliced *XBP1),* additional eIF2B5 depletion induced only the ISR (Extended Data 3h,i) [34].

ATF4 controls transcription of multiple stress-related genes, including *GADD34* and *ATF3*, both of which were induced upon eIF2B5 knockdown in APC^{def}, but not in APC^{res} cells (Fig. 3h and Extended Data 3i). ATF3 is important for CHOP expression [35] and CHOP can drive apoptosis, eliminating cells after prolonged stress [36]. eIF2B5 depletion in APC^{def} cells induced CHOP expression to a similar extent as exposure to tunicamycin (Extended Data 4a), which blocks protein glycosylation and is an established inducer of an ISR [36]. These responses were attenuated in APC^{res} cells (Extended Data 4a). siRNA-mediated CHOP knockdown abolished its upregulation after eIF2B5 depletion in APC^{def} cells, but had only minor effects on the apoptotic response after eIF2B5 depletion (Extended Data 4b,c).

APC loss strongly enhances expression of *MYC* mRNA [9]. Since high MYC levels induce apoptosis [37], we tested whether MYC expression is differentially regulated after eIF2B5 knockdown. Upon eIF2B5 knockdown in APC^{def} cells, MYC protein levels were markedly upregulated, while *MYC* mRNA levels and protein stability remained unaltered (Fig. 4a and Extended Data 4d,e). MYC protein levels were also induced by sh*EIF2B5* #1, but not by sh*EIF2B5* #4 (Extended Data 4f,g). Similarly, MYC is upregulated after eIF2B5 knockdown in APC-deficient HT29 cells, but not in APC-proficient HCT116 cells (Extended Data 4h). Immunoprecipitation of ^{35}S-methionine pulse-labelled MYC showed that eIF2B5 depletion enhanced MYC translation in APC^{def} cells (Fig. 4b). In apoptotic cells, translation of MYC is enhanced via an internal ribosomal entry site (IRES) [38, 39]. A specific inhibitor of MYC IRES-dependent translation, cymarine [40], decreased basal MYC expression and abolished its upregulation in response to eIF2B5 depletion in APC^{def} cells , but had no effect on two other short-lived proteins (Cyclin E, c-Fos) (Fig. 4c and Extended Data 5a). Furthermore, deleting an internal part of the MYC IRES by CRISPR/Cas9 abolished MYC induction upon eIF2B5 knockdown (Extended Data 5b,c,d). We concluded that depletion of eIF2B5 enhances IRES-dependent translation of MYC.

Depletion of MYC strongly reduced induction of apoptosis in response to eIF2B5 depletion in APC^{def} cells (Fig. 4d,e). It also decreased basal CHOP levels and compromised CHOP, *ATF3* and *GADD34* induction upon eIF2B5 knockdown (Fig. 4d and Extended Data 5e). We concluded that eIF2B5 downregulation increases MYC translation in APC^{def} cells, causing apoptosis. Since *MYC* mRNA and the ISR levels, which enhance MYC IRES translation, are lower in APC^{res} cells, eIF2B5 depletion does not cause a similar MYC upregulation in these cells.

To understand how deregulation of protein synthesis and MYC expression contribute to apoptosis, we determined intracellular amino acid pools. Knockdown of eIF2B5 significantly reduced alanine, aspartate and glutamate levels (Fig. 5a). APC restoration or MYC depletion alleviated the effects of eIF2B5 depletion on aspartate and glutamate levels. Both amino acids are precursors for nucleotide synthesis, a highly energy-demanding process [41]. The corresponding biosynthetic enzymes are encoded by MYC target genes and several are induced following *APC* loss (Fig. 5b) [42]. Intriguingly, eIF2B5 depletion decreased tri-phosphorylated nucleotides in APC^{def} cells, which was lessened or abolished by APC restoration, indicative of a reduction in cellular energy charge (Fig. 5c). Consistent with these findings, eIF2B5 depletion strongly increased phosphorylated AMPK in APC^{def}, but not in APC^{res} cells (Fig. 5d). We concluded that eIF2B5 depletion causes an APC-dependent perturbation of cellular amino acid and nucleotide pools and of energy homeostasis.

Physiological eIF2B5 levels are required for tumourigenesis driven by loss of APC

To demonstrate the effects of eIF2B5 depletion in a genetically defined setting, we used intestinal organoids [43, 44], generated from wild-type, *VillinCre*^{ER}*Apc*$^{fl/fl}$ or *VillinCre*^{ER}*Apc*$^{fl/fl}$*Kras*$^{G12D/+}$ mice and recombined them *ex vivo* by addition of 4-hydroxytamoxifen (4-OHT). Accordingly, MYC protein was induced in Cre-recombined organoids relative to wild-type counterparts (Extended Data 6a). Doxycycline-inducible eIF2B5 knockdown had no effect on the size of wild-type organoids, but dramatically reduced

the growth of *VillinCre*^{ER}*Apc*$^{fl/fl}$ and *VillinCre*^{ER}*Apc*$^{fl/fl}$*Kras*$^{G12D/+}$ organoids (Extended Data 6b,c,d), arguing that eIF2B5 levels are critical for the growth of *Apc*-deleted organoids. To validate our findings in a human setting, we used a panel of six patient-derived CRC organoids. All five *APC*-mutated organoids showed a reduction in viability after eIF2B5 knockdown, whereas one *APC* wild-type organoid did not (Extended Data 6e,f,g).

Since a complete *Eif2b5* knockout is embryonically lethal [26], we characterized mice, in which one *Eif2b5* allele has been disrupted by integration of a gene-trap vector generating *Eif2b5*$^{+/tm1a(EUCOMM)Wtsi}$ mice, hereafter designated *Eif2b5*$^{+/-}$ (Extended Data 7a). *Eif2b5*$^{+/-}$ mice were born viable, at normal Mendelian ratios, were phenotypically indistinguishable from their *Eif2b5*$^{+/+}$ littermates and displayed normal intestinal tissue architecture with no changes in cell size, survival, proliferation or differentiation (Extended Data 7b). Relative to wild-type littermates, *Eif2b5*$^{+/-}$ mice displayed an approximately 50% reduction in eIF2B5 protein levels in all analysed organs as well as in intestinal epithelial extracts (Fig. 6a and Extended Data 7c). These findings demonstrate that a 50% reduction in eIF2B5 is compatible with normal organismal development and physiology.

To determine whether eIF2B5 levels are critical for colorectal tumour development driven by *Apc* loss, we used mice carrying the conditional knockout *Apc*^{580s} allele alone or in combination with a conditional allele encoding oncogenic *Kras*^{G12D} (*VillinCre*^{ER}*Apc*$^{fl/fl}$ or *VillinCre*^{ER}*Apc*$^{fl/fl}$*Kras*$^{G12D/+}$) [9, 45-47]. *Apc* deletion and *Kras* mutation increased eIF2B5 protein levels more than two-fold in small intestinal epithelial extracts, similar to what we observed in human tumours (Fig. 6b). Histological staining confirmed reduced expression of eIF2B5 in intestinal epithelia of *Eif2b5*$^{+/-}$ mice (Fig. 6c and Extended Data 7d). Levels of p-eIF2α were low in crypts in wild-type epithelia of small intestine and colon, whereas p-eIF2α was clearly detectable upon *Apc* deletion with or without activation of *Kras*^{G12D}, consistent with previous data that eIF2α phosphorylation increases during tumourigenesis (Fig. 6c and Extended Data 7d) [28]. In both genetic backgrounds, p-eIF2α staining intensity was reduced in *Eif2b5*$^{+/-}$ mice relative to *Eif2b5*$^{+/+}$ counterparts, supporting the tissue culture data (Fig. 6c

and Extended Data 7d). Loss of *Apc* led to massive tissue growth and a corresponding increase in BrdU incorporation in the intestine of *Eif2b5*$^{+/+}$ mice, which were further enhanced upon simultaneous activation of oncogenic *Kras*^{G12D} (Fig. 6c,d and Extended Data 7d,e). These effects were significantly suppressed in the intestine of *Eif2b5*$^{+/-}$ mice, both in the absence or presence of oncogenic *Kras*^{G12D} (Fig. 6c,d and Extended Data 7d,e). Cleaved caspase 3 increased robustly in *VillinCre*^{ER}*Apc*$^{fl/fl}$*Eif2b5*$^{+/-}$ and *VillinCre*^{ER}*Apc*$^{fl/fl}$*Kras*^{G12D}*Eif2b5*$^{+/-}$ compared to their *Eif2b5*$^{+/+}$ counterparts (Fig. 6c,d and Extended Data 7d,e). Loss of *Apc* increases MYC levels which are further enhanced by introduction of a *Kras*^{G12D} allele in *Eif2b5*$^{+/+}$ mice [9, 48]. While corresponding *Eif2b5*$^{+/-}$ mice show a further increase of MYC-positive cells, this did not reach statistical significance (Fig. 6c,d and Extended Data 7d,e). Therefore, the basic mechanism we describe also operates in these cells; possibly, other ISR target proteins contribute to apoptosis induction aside from MYC.

To analyse the impact of eIF2B5 on long-term survival in an *Apc*-deficient mouse model, we crossed *Apc*$^{Min/+}$ [49] mice to *Eif2b5*$^{+/-}$ animals. Relative to *Apc*$^{Min/+}$ littermates, *Apc*$^{Min/+}$*Eif2b5*$^{+/-}$ animals had a significantly extended lifespan (median survival: 149 versus 127.5 days; Extended Data 8a,b). Importantly, organoids established from outgrowing tumours of both genotypes revealed no difference in p-eIF2α levels, protein synthesis rates and polysome/sub-polysome ratio (Extended Data 8c-f). Furthermore, *Eif2b5*$^{+/-}$ tumours restored eIF2B5 expression to approximately 70% of wild-type levels, indicating that significant compensation had taken place during tumour evolution (Extended Data 8c,d).

Finally, acute deletion of both alleles of *Eif2b5* in *VillinCre*^{ER}*Apc*$^{fl/fl}$ mice decreased cell proliferation and concomitantly increased MYC expression (Extended Data 8g,h), confirming that targeting eIF2B5 can strongly affect tumour growth and raising the possibility that MYC translation is largely independent of eIF2B5 *in vivo*.

Targeting PKR and GCN2 opens a therapeutic window for APC loss-driven CRC

Since eIF2B5 cannot currently be targeted by small molecules, we tested whether inhibiting eIF2α phosphorylation can achieve similar therapeutic efficacy. Four kinases (EIF2AK1-4) phosphorylate eIF2α in response to distinct stresses [50]. Of these, HRI (heme-regulated inhibitor; EIF2AK1) restricts globin translation in erythrocytes upon heme depletion, and PERK (EIF2AK3) is activated in response to ER stress (see above). We therefore focused on PKR (EIF2AK2), activated by double-stranded RNA, and on GCN2 (EIF2AK4), activated by depletion of amino acids and uncharged tRNA pools [50]. Using antibodies that detect the phosphorylated, active forms, we found that GCN2 and, to a lesser degree, PKR are activated in APC^{def} compared to APC^{res} cells (Fig. 7a). Intriguingly, MYC knockdown reduced the levels of phosphorylated PKR and essentially abolished GCN2 phosphorylation (Fig. 7a and Extended Data 9a).

Individual PKR or GCN2 knockdown suppressed the growth of APC^{def} cells to a variable extent (Extended Data 9b). However, genetic depletion of either GCN2 or PKR did not decrease p-eIF2α levels (Extended Data 9c), arguing that cells compensate for the lack of either kinase during genetic suppression. To test whether an acute inhibition of either kinase activity can mimic eIF2B5 depletion, we used small molecule inhibitors of GCN2 (A-92), PKR (C16), or PERK (GSK2606414, hereafter GSK'414) [50]. GCN2 or PKR inhibition suppressed the growth of APC^{def} cells, but had only minor effects on APC^{res} cells (Fig. 7b). Both inhibitors induced apoptosis in a dose-dependent manner in APC^{def} cells, but to a much lesser degree in APC^{res} cells, whereas inhibition of PERK had minor to no effects (Fig. 7c). In addition, A-92 reduced p-eIF2α levels, increased protein synthesis rates and induced MYC expression in APC^{def} cells, thereby phenocopying the effects of eIF2B5 depletion (Fig. 7d,e). These effects were less pronounced in response to PKR inhibition (Fig. 7f,g). Importantly, treatment of *VillinCre*^{ER}*Apc*$^{fl/fl}$ or *VillinCre*^{ER}*Apc*$^{fl/fl}$*Kras*$^{G12D/+}$ organoids with GCN2 or PKR inhibitors suppressed organoid viability, whereas wild-type organoids were not affected (Fig. 8a,b). Similarly, eight APC-mutated patient-derived organoid lines were sensitive to GCN2 and PKR inhibition (Fig. 8c,d and Extended Data 10a). Furthermore, both inhibitors reduced p-

323 eIF2α levels in three human organoid lines, validating their on-target activity (Extended Data
324 10b). Finally, combining inhibitors with shRNAs that deplete the kinase not targeted by the
325 inhibitor led to additive effects in apoptosis induction (Extended Data 10c). We concluded
326 that primarily inhibition of GCN2, and to a lesser extent PKR, phenocopies eIF2B5 depletion
327 and suppresses the growth of APC-mutated CRC.
328

Discussion

Loss of *APC* increases global translation rates, leading to a MYC-dependent transcriptional upregulation of multiple genes encoding proteins involved in mRNA translation. Using a newly-established APC-deficient CRC cell line that can be induced to re-express full-length APC, we uncovered a negative feedback loop which limits protein synthesis to prevent MYC-dependent apoptosis. We show that this is a vulnerability of APC-deficient CRC cells that can be targeted using small molecules.

Specifically, we found that the survival of APC-deficient cells strictly depends on physiological levels of the translation initiation factor eIF2B5. eIF2B5 depletion reduces the initiation of mRNA translation leading to an ISR that involves a stress-related translation program. In parallel, eIF2B5 depletion enhances MYC translation via a stress-responsive IRES in the 5'-UTR of the *MYC* mRNA. Induction of apoptosis upon eIF2B5 depletion depends on MYC upregulation; other proteins translated as part of the ISR may also contribute. In culture, eIF2B5 depletion induces apoptosis selectively in APC-deficient cells since loss of APC upregulates *MYC* mRNA levels [8]. Accordingly, *Eif2b5*$^{+/-}$ mice show a normal development but a strongly impaired hyperproliferation in response to *Apc* loss correlating with increased apoptosis.

The eIF2B complex binds tightly to eIF2 when eIF2α is phosphorylated [24], preventing dephosphorylation of eIF2α. In tumour cells, a significant fraction of eIF2α is phosphorylated and hence tightly bound to eIF2B. As a consequence, eIF2B5 depletion leads to increased rather than decreased, overall protein synthesis rates. This increase, in combination with a MYC-driven induction of genes encoding nucleotide biosynthesis enzymes, causes an imbalance in amino acid and nucleotide pools and strains cellular energy resources, leading to activation of AMPK upon eIF2B5 depletion in APC-deficient cells. Activation of AMPK is a critical mediator of MYC-driven apoptosis in epithelial cells [51, 52], suggesting that it contributes to MYC-dependent apoptosis upon eIF2B5 depletion.

Deregulated protein synthesis and the perturbance of amino acid pools activate the GCN2 kinase, which binds uncharged tRNAs in response to decreased amino acid levels and phosphorylates eIF2α [53]. Deregulation of MYC broadly stimulates RNA synthesis by all three RNA polymerases [17], suggesting that GCN2 provides a negative feedback signal that restricts MYC translation to couple MYC-driven RNA synthesis to the availability of amino acids (Fig. 8e). This notion is supported by previous observations implicating GCN2 in the control of MYC translation [54]. MYC also contributes to the activation of PKR and inhibition of PKR partially mimics the phenotype of GCN2 inhibition. Importantly, small molecule inhibitors of GCN2 and, to a lesser degree, of PKR phenocopies eIF2B5 depletion, arguing that inhibitors of either kinase are valid tools for the therapy of APC-deficient CRC. Since transcription of *MYC* is almost universally deregulated in human tumours, strategies that disrupt the negative MYC/GCN2/eIF2α feedback loop to induce apoptosis may be broadly applicable in human tumours.

Acknowledgements

This study was supported by grants from the Else-Kröner-Fresenius Foundation (2015_A57 to A.W.), the interdisciplinary center for clinical research of the Medical Faculty Würzburg (IZKF B-186 and B-335 to A.W.), European Research Council Grants “AuroMYC” (Advanced Grant to M.E.) and "ColonCan" (Starting Grant to O.J.S; 311301), a Cancer Research UK Grand Challenge grant (A25045 to O.J.S.), Cancer Research UK core funding (A17196 and A21139 to O.J.S) and the Deutsche Forschungsgemeinschaft (DFG) (WO 2108/1-1 to E.W., FOR2314 and KFO DFG EI 222/8-1 grants to M.E., FOR2314 and KFO DFG WI 5037/2-2 to A.W.) and the Wilhelm Sander-Stiftung (to M.E). S.W. is supported by the Comprehensive Cancer Center program of the German Cancer Aid (Deutsche Krebshilfe). Additional personal financial support was given by Mr. Kratz. The technical expertise of Sabine Roth, Barbara Bauer, Hecham Marouf and Cornelius Schneider is gratefully acknowledged. The invaluable support of the Histology Service, the Biological Services Unit, and all the core services at the Cancer Research UK Beatson Institute is greatly appreciated (Cancer Research UK core grant C596/A17196).

Author contributions

S.S., D.G., F.W.U., O.J.S, M.E. and A.W. conceived the project and directed experiments. Experiments were performed by S.S., D.G., F.W.U., S.D., M.P., N.M., S.B., C.F., F.C.W., C.P.A., A.B., R.J., C.S.-V., K.M., W.S., J.R.P.K., D.S., A.R. and A.W. Data were analysed and interpreted by S.S., D.G., F.W.U., S.D., M.P., C.P.A., F.E., W.S., E.W., A.S., A.R., O.J.S., M.E., A.W. Bioinformatical analysis was done by F.W.U., C.P.A., S.W. and F.E. Administrative, technical, or material support was given by M.E.D., S.B., F.C.W., G.V., N.V., C.O., E.W., D.S., C.-T.G., A.R., O.J.S. and M.E. S.S., D.G., E.W., C.-T.G., O.J.S., M.E. and A.W. wrote the manuscript. All authors reviewed and approved the manuscript.

Competing Interests

399 The authors declare no competing interests.

400

401

Figure legends

Figure 1: Restoration of APC expression suppresses translation and anchorage-independent growth.

(**a**) Immunoblot of SW480^{TetOnAPC} cells after 48 h treatment with doxycycline (APC^{res}) or ethanol (APC^{def}), representative of three independent experiments with similar results.

(**b**) mRNA expression of *APC* in SW480^{TetOnAPC} cells (96 h ethanol or doxycycline, respectively) analysed via qPCR (n = 3 biologically independent experiments); unpaired, two-tailed *t*-test.

(**c**) mRNA expression of WNT pathway target genes *MYC*, *AXIN2*, *DKK1* in SW480^{TetOnAPC} cells treated as described in (**b**) analysed via qPCR (n = 3 biologically independent experiments); unpaired, two-tailed *t*-test.

(**d**) RNA-sequencing followed by GSEA of gene expression changes in APC^{def} and APC^{res} cells (48 h ethanol and doxycycline, respectively). Enrichment plots of indicated gene sets are displayed (n = 3 biologically independent experiments). Calculation of the normalised enrichment score (NES) is based on a weighted running sum statistic and computed as part of the GSEA methodology [55]. A Kolmogorov-Smirnov test with 1,000 permutations was used to calculate *P* values that were then corrected for multiple testing using the Benjamini-Hoechberg procedure (FDR).

(**e**) ^{35}S-methionine labelling of APC^{def} and APC^{res} cells (72 h doxycycline). Incorporated radioactivity was measured by scintillation counting. Data show mean ± s.d. (n = 3 biologically independent experiments); unpaired, two-tailed *t*-test.

(**f**) Cumulative growth curve of APC^{def} and APC^{res} cells treated with doxycycline or ethanol, respectively. Data show mean ± s.d. (n = 3 biologically independent experiments); unpaired, two-tailed *t*-test.

(**g**) Anchorage-independent growth of APC^{def} and APC^{res} colonies. Colonies were grown over ten days, with fresh ethanol or doxycycline added every third day. Representative colonies are shown. Scale bars = 50 μM.

(**h**) Quantification of size of colonies from (**g**). Data show mean ± s.d. of all colonies counted (n = 29 for APC^{def} and n = 25 for APC^{res}); unpaired, two-tailed t-test.

(**i**) Quantification of number of colonies from (**g**). Data show mean ± s.d. (n = 3 biologically independent experiments); unpaired, two-tailed t-test.

Unprocessed immunoblots are shown in Source Data Figure 1.

Figure 2: APC-deficient CRC cells depend on physiological eIF2B5 levels.

(**a**) Plot documenting $\log_2$ fold change of all shRNAs included in the screen in APC^{res} versus APC^{def} cells (median of n = 3 biologically independent experiments) with five shRNAs targeting *EIF2B5* shown in colour.

(**b**) Crystal violet staining of shCTR-transduced or eIF2B5-depleted APC^{def} and APC^{res} cells (six days ethanol and doxycycline, respectively), representative of three biologically independent experiments with similar results. Cells were lentivirally infected with shRNAs targeting *EIF2B5* or luciferase (shCTR).

(**c**) Relative number of shCTR-transduced or eIF2B5-depleted APC^{def} and APC^{res} cells (seven days ethanol or doxycycline, respectively). Cell numbers were determined by staining with Hoechst and high-content microscopy imaging. Data show mean ± s.d. (n = 3 biologically independent experiments); unpaired, two-tailed t-test.

(**d**) Immunoblot of shCTR-transduced or eIF2B5-depleted APC^{def} and APC^{res} cells (72 h ethanol or doxycycline), representative of five independent experiments with similar results.

(**e**) *EIF2B5* mRNA levels determined via qPCR from cells described in (**d**). Data show mean ± s.d. (n = 4 biologically independent experiments); unpaired, two-tailed t-test.

(**f**) Annexin V/PI FACS analysis of shCTR-transduced or eIF2B5-depleted APC^{def} and APC^{res} cells (96 h ethanol or doxycycline, respectively). Data shown mean ± s.d. (n = 3 biologically independent experiments); unpaired, two-tailed t-test.

(**g**) Immunoblot of shCTR-transduced or eIF2B5-depleted HT29 and HCT116 cells, representative of two independent experiments with similar results. Cells were lentivirally infected with shRNAs targeting *EIF2B5* or luciferase (shCTR).

(**h**) Crystal violet staining of shCTR-transduced or eIF2B5-depleted HT29 and HCT116 cells, representative of two independent experiments with similar results.

(**i**) eIF2B5 staining of human CRC tumour tissue and normal mucosa (representative image of *n* = 10 biologically independent patients). Scale bars = 100 µm.

Unprocessed immunoblots are shown in Source Data Figure 2.

Figure 3: eIF2B5 controls translation initiation and limits global protein synthesis.

(**a**) Polysome profiling of shCTR-transduced and eIF2B5-depleted APC^{def} cells (72 h ethanol) incubated with harringtonine for 0 s (left) and 180 s (right) before harvest. 40S, 60S, 80S monosomal and polysomal fractions are indicated. Data (0 s harringtonine) are representative of three independent experiments with similar results, 180 s harringtonine assay was performed once.

(**b**) ^{35}S-methionine labelling of shCTR-transduced and eIF2B5-depleted APC^{def} and APC^{res} cells (72 h ethanol or doxycycline, respectively). Incorporated radioactivity was measured by scintillation counting. Data show mean ± s.d. (*n* = 3 biologically independent experiments); unpaired, two-tailed *t*-test.

(**c**) Total eIF2α and p-eIF2α S51 staining of human CRC tumour tissue and normal mucosa (representative image of *n* = 10 biologically independent patients). Scale bars = 100 µm.

(**d**) Immunoblot of shCTR-transduced and eIF2B5-depleted APC^{def} and APC^{res} cells (96 h ethanol or doxycycline, respectively), representative of three independent experiments with similar results. p-eIF2α S51 levels, relative to total eIF2α levels, are shown below the immunoblot.

(**e**) Immunoprecipitation of eIF2α in shCTR-transduced or eIF2B5-depleted APC^{def} and APC^{res} cells (72 h ethanol or doxycycline, respectively). As input, 3% of lysate was loaded. Proteins bound to eIF2α were detected by immunoblotting. Average levels of immunoprecipitated PP1 relative to immunoprecipitated eIF2α levels, normalised to input, are shown below (*n* = 2 biologically independent experiments). s.e. short exposition, l.e. long exposition.

(**f**) Immunoblot of shCTR-transduced or eIF2B5-depleted APC^{def} and APC^{res} cells treated as described in (**d**), representative of three independent experiments with similar results.

(**g**) RNA-sequencing followed by GSEA of gene expression changes in shCTR-transduced or eIF2B5-depleted APC^{def} cells. Enrichment plot of a Reactome gene set representing an ATF4-dependent stress response is shown (n = 3 biologically independent experiments). Statistical analysis was done as described in Fig. 1d.

(**h**) Immunoblot of shCTR-transduced or eIF2B5-depleted APC^{def} and APC^{res} cells treated as described in (**d**), representative of three independent experiments with similar results.

Unprocessed immunoblots are shown in Source Data Figure 3.

Figure 4: Depletion of eIF2B5 causes MYC-driven apoptosis.

(**a**) Immunoblot of shCTR-transduced or eIF2B5-depleted APC^{def} and APC^{res} cells (96 h ethanol or doxycycline, respectively), representative of three independent experiments with similar results.

(**b**) ^{35}S-methionine pulse-labelling followed by immunoprecipitation with a MYC-specific antibody or control IgG in shCTR-transduced or eIF2B5-depleted APC^{def} and APC^{res} cells (96 h ethanol or doxycycline, respectively). Protein synthesis inhibitor cycloheximide (CHX) was used as control. Radio-labelled MYC was detected by autoradiography. The arrow indicates the position of the specific MYC band. Average MYC levels are shown below the panel (n = 3 biologically independent experiments).

(**c**) Immunoblot of cymarine-treated (100 nM, 24 h) shCTR-transduced or eIF2B5-depleted APC^{def} and APC^{res} cells (72 h ethanol or doxycycline, respectively), representative of two independent experiments with similar results. DMSO was used as solvent control.

(**d**) Immunoblot of shCTR-transduced and eIF2B5-depleted APC^{def} and APC^{res} cells (96 h ethanol or doxycycline, respectively) upon MYC depletion, representative of two independent experiments with similar results. siRNA transfections were carried out using siCTR as non-targeting control or si*MYC* for 72 h.

(**e**) Annexin V/PI FACS of shCTR-transduced or eIF2B5-depleted APC^{def} and APC^{res} cells treated as described in (**d**). Data show mean ± s.d. (n = 3 biologically independent experiments), unpaired, two-tailed *t*-test.

Unprocessed immunoblots are shown in Source Data Figure 4.

Figure 5: Depletion of eIF2B5 causes an imbalance in amino acid and nucleotide pools.

(**a**) Mass spectrometric analysis of intracellular alanine, aspartate and glutamate levels in shCTR-transduced or eIF2B5-depleted APC^{def} and APC^{res} cells upon MYC depletion. siRNA transfections were carried out using siCTR as non-targeting control or si*MYC* for 72 h. Relative measured peak area normalised to protein concentration and total amino acid levels is shown. Peak area in APC^{def} cells transfected with siCTR was set to one. Data represent mean + s.d. (n = 6 biologically independent experiments); unpaired, two-tailed *t*-test.

(**b**) MA plot of RNA-sequencing data of APC^{def} and APC^{res} cells. Genes associated with inosine monophosphate (IMP)/purine biosynthesis (GO:0006188) are highlighted in red (n = 3 biologically independent experiments).

(**c**) Mass spectrometric analysis of intracellular nucleotide levels in shCTR-transduced and eIF2B5-depleted APC^{def} and APC^{res} cells treated as described in (**a**). Relative measured peak area normalised to protein concentration is shown. Peak area in APC^{def} cells transfected with siCTR was set to one. Data represent mean + s.d. (n = 5 biologically independent experiments); unpaired, two-tailed *t*-test.

(**d**) Immunoblot of shCTR-transduced or eIF2B5-depleted APC^{def} and APC^{res} cells (96 h ethanol or doxycycline, respectively), representative of two independent experiments with similar results. As control for AMPK activation, cells were treated with AICAR (1 mM, 24 h).

Unprocessed immunoblots are shown in Source Data Figure 5.

Figure 6: Physiological eIF2B5 levels are required for tumourigenesis driven by loss of *Apc*.

(**a**) Immunoblot of small intestine (s.i.), colon, liver, spleen and kidney from wild-type and *Eif2b5*$^{+/-}$ mice. Analysis was done once with one mouse per genotype.

(**b**) Immunoblot of intestinal epithelial extracts from mice of the indicated genotypes (left). Each lane represents one separate mouse of the relevant group. Immunoblot was performed once. Quantification of eIF2B5 protein levels, normalised to γ-tubulin (right). Data show mean ± s.d. (*n* = 3 biologically independent mice); one-tailed Mann-Whitney *U* test.

(**c**) Representative H&E-, eIF2B5-, p-eIF2α S51-, BrdU-, cleaved caspase 3-, and MYC-stained sections of small intestines from mice of the indicated genotypes. Mice were sampled four and three days post-induction, as described in Methods. Red bars indicate the length of the crypt (top panel). Scale bars = 100 μm.

(**d**) Graphs documenting the position of the highest BrdU-positive cell along the crypt-villus axis (top panel), the total number of cells staining positive for BrdU per half crypt (top middle panel), and the total number of cells per full crypt staining positive for cleaved caspase 3 (bottom middle panel) or MYC (bottom panel) in small intestines from mice of the indicated genotypes. Data were scored in 25 crypts per mouse in at least three biologically independent mice (*n* = 3 for highest BrdU-positive cell in wild-type and *Eif2b5*$^{+/-}$, *n* = 5 for highest BrdU-positive cell in *VillinCre*^{ER}*Apc*$^{fl/fl}$*Eif2b5*$^{+/-}$, *n* = 5 for BrdU staining in *VillinCre*^{ER}*Apc*$^{fl/fl}$*Eif2b5*$^{+/-}$, *n* = 5 for cleaved caspase 3 staining in *VillinCre*^{ER}*Apc*$^{fl/fl}$*Eif2b5*$^{+/-}$ and *VillinCre*^{ER}*Apc*$^{fl/fl}$*Kras*$^{G12D/+}$*Eif2b5*$^{+/-}$, *n* = 5 for MYC staining in *Eif2b5*$^{+/-}$, *VillinCre*^{ER}*Apc*$^{fl/fl}$ and *VillinCre*^{ER}*Apc*$^{fl/fl}$*Eif2b5*$^{+/-}$ mice, *n* = 6 for all other stainings and genotypes). Data show mean ± s.e.m.; one-tailed Mann-Whitney *U*.

Unprocessed immunoblots are shown in Source Data Figure 6.

Figure 7: Inhibition of PKR and GCN2 phenocopies eIF2B5 knockdown.

(**a**) Immunoblot of APC^{def} and APC^{res} cells upon siRNA-mediated knockdown of MYC (96 h ethanol or doxycycline, respectively), representative of two independent experiments with similar results. siRNA transfections were carried out using siCTR as non-targeting control or si*MYC* for 72 h.

(**b**) Crystal violet staining of APC^{def} and APC^{res} cells (seven days ethanol or doxycycline, respectively) in the presence of the following eIF2α kinase inhibitors for 96 h: A-92 (GCN2

inhibitor), C16 (PKR inhibitor), GSK2606414 (PERK inhibitor, designated GSK‘414), representative of three independent experiments with similar results. DMSO was used as solvent control.

(**c**) Annexin V/PI FACS analysis of APC^{def} and APC^{res} cells (five days ethanol or doxycycline, respectively) treated with DMSO or inhibitors of GCN2 (A-92), PKR (C16), or PERK (GSK'414) for 48 h at the indicated concentrations. Data show mean ± s.d. (*n* = 3 biologically independent experiments); unpaired, two-tailed *t*-test.

(**d**) Immunoblot of APC^{def} and APC^{res} cells (72 h ethanol or doxycycline, respectively) after DMSO or A-92 treatment (2 h), representative of two independent experiments with similar results. p-eIF2α S51 levels, relative to total eIF2α levels, are shown below the immunoblot.

(**e**) ^{35}S-methionine labelling of APC^{def} and APC^{res} cells (96 h ethanol or doxycycline, respectively) treated with DMSO or GCN2 inhibitor A-92 for 48 h. Incorporated radioactivity was measured by scintillation counting. Data show mean ± s.e.m. (*n* = 3 biologically independent experiments); unpaired, two-tailed *t*-test.

(**f**) Immunoblots of APC^{def} and APC^{res} cells (72 h ethanol or doxycycline, respectively) after DMSO or C16 treatment (2 h), representative of two independent experiments with similar results. p-eIF2α S51 levels, relative to total eIF2α levels, are shown below the immunoblot.

(**g**) ^{35}S-methionine labelling of APC^{def} and APC^{res} cells (96 h ethanol or doxycycline, respectively) treated with DMSO or PKR inhibitor C16 for 48 h. Incorporated radioactivity was measured by scintillation counting. Data show mean ± s.e.m. (*n* = 3 biologically independent experiments); unpaired, two-tailed *t*-test.

Unprocessed immunoblots are shown in Source Data Figure 7.

Figure 8: Targeting PKR and GCN2 activity opens a therapeutic window in *APC*-loss driven CRC.

(**a**) Growth of murine organoids upon GCN2, PKR or PERK inhibition. Wild-type, *VillinCre*^{ER}*Apc*$^{fl/fl}$ or *VillinCre*^{ER}*Apc*$^{fl/fl}$*Kras*$^{G12D/+}$ organoids were grown for 72 h, then treated

596 with A-92, C16 or GSK‘414 for 72 h. DMSO was used as solvent control. Representative
597 pictures of one organoid line of each genotype. Scale bars = 200 µM.
598 (**b**) Viability of organoids treated as described in (**a**) assessed using CellTiter Blue assay.
599 Data show mean of at least four technical replicates (black dots) of one line each,
600 representative of two biologically independent organoid lines per genotype and experiments
601 with similar results.
602 (**c**) Growth of one patient-derived organoid line treated with GCN2 (A-92) or PKR (C16)
603 inhibitors. T4 organoid line was grown for two days, and then treated with DMSO, A-92 or
604 C16 for 96 h at the indicated concentrations. Representative pictures from one experiment
605 are shown. Scale bars = 200 µM.
606 (**d**) Quantification of viability of eight patient-derived CRC organoid lines assessed by
607 CellTiter Blue assay. Organoids were treated as described in (**c**). Data show mean ± s.e.m
608 (*n* = 8 independent organoid lines; T1, T2, T3, T4, T5, T11, T13, T15); unpaired, two-tailed *t*-
609 test.
610 (**e**) Model explaining our findings. A MYC/GCN2/eIF2α negative feedback loop limits protein
611 synthesis to prevent MYC-dependent apoptosis in APC-deficient cells. In APC-proficient
612 cells, transcription of the *MYC* gene is strongly suppressed, hence the dependence on this
613 negative feedback loop is not shown.
614

615 **References**

616 1. Truitt, M.L., et al., *Differential Requirements for eIF4E Dose in Normal Development*
617 *and Cancer.* Cell, 2015. **162**(1): p. 59-71.
618 2. Jackson, R.J., C.U. Hellen, and T.V. Pestova, *The mechanism of eukaryotic*
619 *translation initiation and principles of its regulation.* Nat Rev Mol Cell Biol, 2010. **11**(2): p.
620 113-27.
621 3. Pakos-Zebrucka, K., et al., *The integrated stress response.* EMBO Rep, 2016. **17**(10):
622 p. 1374-1395.
623 4. Jennings, M.D., et al., *Fail-safe control of translation initiation by dissociation of*
624 *eIF2alpha phosphorylated ternary complexes.* Elife, 2017. **6**.
625 5. Kenner, L.R., et al., *eIF2B-catalyzed nucleotide exchange and phosphoregulation by*
626 *the integrated stress response.* Science, 2019. **364**(6439): p. 491-495.
627 6. Adomavicius, T., et al., *The structural basis of translational control by eIF2*
628 *phosphorylation.* Nat Commun, 2019. **10**(1): p. 2136.
629 7. CancerGenomeAtlasNetwork, *Comprehensive molecular characterization of human*
630 *colon and rectal cancer.* Nature, 2012. **487**(7407): p. 330-7.
631 8. van de Wetering, M., et al., *The beta-catenin/TCF-4 complex imposes a crypt*
632 *progenitor phenotype on colorectal cancer cells.* Cell, 2002. **111**(2): p. 241-50.
633 9. Sansom, O.J., et al., *Myc deletion rescues Apc deficiency in the small intestine.*
634 Nature, 2007. **446**(7136): p. 676-9.
635 10. Dow, L.E., et al., *Apc Restoration Promotes Cellular Differentiation and Reestablishes*
636 *Crypt Homeostasis in Colorectal Cancer.* Cell, 2015. **161**(7): p. 1539-1552.
637 11. Faller, W.J., et al., *mTORC1-mediated translational elongation limits intestinal tumour*
638 *initiation and growth.* Nature, 2015. **517**(7535): p. 497-500.
639 12. Truitt, M.L. and D. Ruggero, *New frontiers in translational control of the cancer*
640 *genome.* Nat Rev Cancer, 2017. **17**(5): p. 332.
641 13. Truitt, M.L. and D. Ruggero, *New frontiers in translational control of the cancer*
642 *genome.* Nat Rev Cancer, 2016. **16**(5): p. 288-304.
643 14. Barna, M., et al., *Suppression of Myc oncogenic activity by ribosomal protein*
644 *haploinsufficiency.* Nature, 2008. **456**(7224): p. 971-5.
645 15. Thoreen, C.C., et al., *A unifying model for mTORC1-mediated regulation of mRNA*
646 *translation.* Nature, 2012. **485**(7396): p. 109-13.
647 16. Wiegering, A., et al., *Targeting Translation Initiation Bypasses Signaling Crosstalk*
648 *Mechanisms That Maintain High MYC Levels in Colorectal Cancer.* Cancer Discov, 2015.
649 **5**(7): p. 768-81.
650 17. Dang, C.V., *MYC on the path to cancer.* Cell, 2012. **149**(1): p. 22-35.
651 18. Sansom, O.J., et al., *Loss of Apc in vivo immediately perturbs Wnt signaling,*
652 *differentiation, and migration.* Genes Dev, 2004. **18**(12): p. 1385-90.
653 19. Willert, J., et al., *A transcriptional response to Wnt protein in human embryonic*
654 *carcinoma cells.* BMC Dev Biol, 2002. **2**: p. 8.
655 20. Bild, A.H., et al., *Oncogenic pathway signatures in human cancers as a guide to*
656 *targeted therapies.* Nature, 2006. **439**(7074): p. 353-7.
657 21. Hanahan, D. and R.A. Weinberg, *Hallmarks of cancer: the next generation.* Cell,
658 2011. **144**(5): p. 646-74.
659 22. Faux, M.C., et al., *Restoration of full-length adenomatous polyposis coli (APC) protein*
660 *in a colon cancer cell line enhances cell adhesion.* J Cell Sci, 2004. **117**(Pt 3): p. 427-39.
661 23. Rosenbluh, J., et al., *beta-Catenin-driven cancers require a YAP1 transcriptional*
662 *complex for survival and tumorigenesis.* Cell, 2012. **151**(7): p. 1457-73.
663 24. Jennings, M.D. and G.D. Pavitt, *A new function and complexity for protein translation*
664 *initiation factor eIF2B.* Cell Cycle, 2014. **13**(17): p. 2660-5.
665 25. Pavitt, G.D., *Regulation of translation initiation factor eIF2B at the hub of the*
666 *integrated stress response.* Wiley Interdiscip Rev RNA, 2018: p. e1491.
667 26. Hart, T., et al., *High-Resolution CRISPR Screens Reveal Fitness Genes and*
668 *Genotype-Specific Cancer Liabilities.* Cell, 2015. **163**(6): p. 1515-26.

27. Fresno, M., A. Jimenez, and D. Vazquez, *Inhibition of translation in eukaryotic systems by harringtonine.* Eur J Biochem, 1977. **72**(2): p. 323-30.
28. Lobo, M.V., et al., *Levels, phosphorylation status and cellular localization of translational factor eIF2 in gastrointestinal carcinomas.* Histochem J, 2000. **32**(3): p. 139-50.
29. Crouch, D. and B. Safer, *The association of eIF-2 with Met-tRNAi or eIF-2B alters the specificity of eIF-2 phosphatase.* J Biol Chem, 1984. **259**(16): p. 10363-8.
30. Ingolia, N.T., et al., *The ribosome profiling strategy for monitoring translation in vivo by deep sequencing of ribosome-protected mRNA fragments.* Nat Protoc, 2012. **7**(8): p. 1534-50.
31. Rubio, C.A., et al., *Transcriptome-wide characterization of the eIF4A signature highlights plasticity in translation regulation.* Genome Biol, 2014. **15**(10): p. 476.
32. Hinnebusch, A.G., *Translational regulation of GCN4 and the general amino acid control of yeast.* Annu Rev Microbiol, 2005. **59**: p. 407-50.
33. Gardner, B.M., et al., *Endoplasmic reticulum stress sensing in the unfolded protein response.* Cold Spring Harb Perspect Biol, 2013. **5**(3): p. a013169.
34. Hetz, C., E. Chevet, and S.A. Oakes, *Proteostasis control by the unfolded protein response.* Nat Cell Biol, 2015. **17**(7): p. 829-38.
35. Jiang, H.Y., et al., *Activating transcription factor 3 is integral to the eukaryotic initiation factor 2 kinase stress response.* Mol Cell Biol, 2004. **24**(3): p. 1365-77.
36. Zinszner, H., et al., *CHOP is implicated in programmed cell death in response to impaired function of the endoplasmic reticulum.* Genes Dev, 1998. **12**(7): p. 982-95.
37. Murphy, D.J., et al., *Distinct thresholds govern Myc's biological output in vivo.* Cancer Cell, 2008. **14**(6): p. 447-57.
38. Shi, Y., et al., *Therapeutic potential of targeting IRES-dependent c-myc translation in multiple myeloma cells during ER stress.* Oncogene, 2016. **35**(8): p. 1015-24.
39. Stoneley, M., et al., *c-Myc protein synthesis is initiated from the internal ribosome entry segment during apoptosis.* Mol Cell Biol, 2000. **20**(4): p. 1162-9.
40. Didiot, M.C., et al., *Identification of cardiac glycoside molecules as inhibitors of c-Myc IRES-mediated translation.* J Biomol Screen, 2013. **18**(4): p. 407-19.
41. Berg, J.M., J.L. Tymoczko, and L. Stryer, *Biochemistry*. Sixth ed. ed. 2007, New York: W. H. Freeman and company. 1 vol. (pagination multiple).
42. Zuber, J., et al., *RNAi screen identifies Brd4 as a therapeutic target in acute myeloid leukaemia.* Nature, 2011. **478**(7370): p. 524-8.
43. van de Wetering, M., et al., *Prospective derivation of a living organoid biobank of colorectal cancer patients.* Cell, 2015. **161**(4): p. 933-45.
44. Sato, T., et al., *Single Lgr5 stem cells build crypt-villus structures in vitro without a mesenchymal niche.* Nature, 2009. **459**(7244): p. 262-5.
45. el Marjou, F., et al., *Tissue-specific and inducible Cre-mediated recombination in the gut epithelium.* Genesis, 2004. **39**(3): p. 186-93.
46. Shibata, H., et al., *Rapid colorectal adenoma formation initiated by conditional targeting of the Apc gene.* Science, 1997. **278**(5335): p. 120-3.
47. Jackson, E.L., et al., *Analysis of lung tumor initiation and progression using conditional expression of oncogenic K-ras.* Genes Dev, 2001. **15**(24): p. 3243-8.
48. Adhikary, S. and M. Eilers, *Transcriptional regulation and transformation by Myc proteins.* Nat Rev Mol Cell Biol, 2005. **6**(8): p. 635-45.
49. Su, L.K., et al., *Multiple intestinal neoplasia caused by a mutation in the murine homolog of the APC gene.* Science, 1992. **256**(5057): p. 668-70.
50. Donnelly, N., et al., *The eIF2alpha kinases: their structures and functions.* Cell Mol Life Sci, 2013. **70**(19): p. 3493-511.
51. Haikala, H.M., et al., *Pharmacological reactivation of MYC-dependent apoptosis induces susceptibility to anti-PD-1 immunotherapy.* Nat Commun, 2019. **10**(1): p. 620.
52. Nieminen, A.I., et al., *Myc-induced AMPK-phospho p53 pathway activates Bak to sensitize mitochondrial apoptosis.* Proc Natl Acad Sci U S A, 2013. **110**(20): p. E1839-48.
53. Castilho, B.A., et al., *Keeping the eIF2 alpha kinase Gcn2 in check.* Biochim Biophys Acta, 2014. **1843**(9): p. 1948-68.

54. Yue, M., et al., *Oncogenic MYC Activates a Feedforward Regulatory Loop Promoting Essential Amino Acid Metabolism and Tumorigenesis.* Cell Rep, 2017. **21**(13): p. 3819-3832.
55. Subramanian, A., et al., *Gene set enrichment analysis: a knowledge-based approach for interpreting genome-wide expression profiles.* Proc Natl Acad Sci U S A, 2005. **102**(43): p. 15545-50.

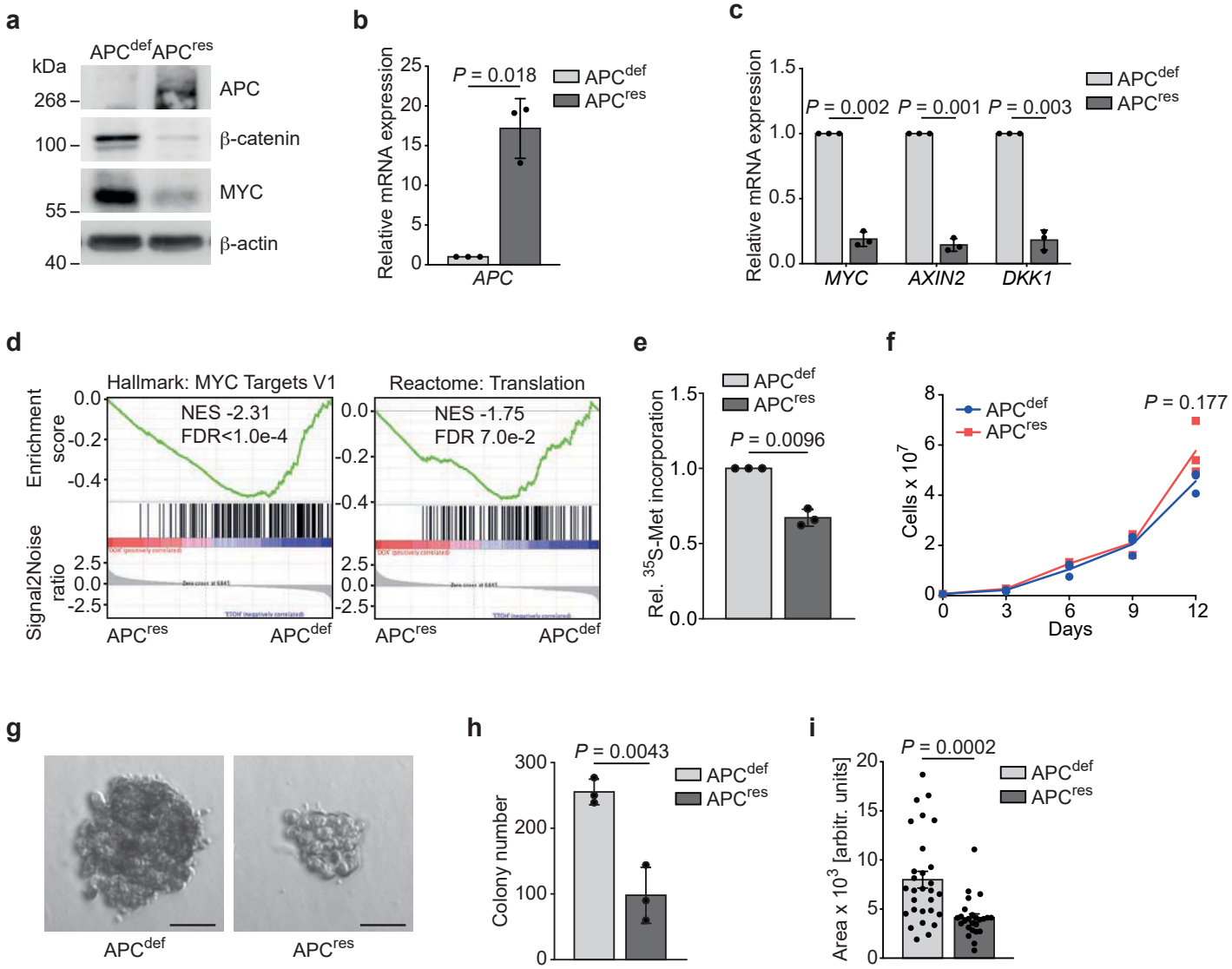
a
APCdefAPCres
kDa
268
100
55
40
APC
β-catenin
MYC
β-actin
b
Relative mRNA expression
P = 0.018
APCdef
APCres
APC
c
Relative mRNA expression
P = 0.002
P = 0.001
P = 0.003
APCdef
APCres
MYC
AXIN2
DKK1
d
Hallmark: MYC Targets V1
NES -2.31
FDR<1.0e-4
Reactome: Translation
NES -1.75
FDR 7.0e-2
Enrichment score
Signal2Noise ratio
APCres
APCdef
e
Rel. 35S-Met incorporation
APCdef
APCres
P = 0.0096
f
Cells x 10^7
APCdef
APCres
P = 0.177
Days
g
APCdef
APCres
h
Colony number
P = 0.0043
APCdef
APCres
i
Area x 10^3 [arbitr. units]
P = 0.0002
APCdef
APCres

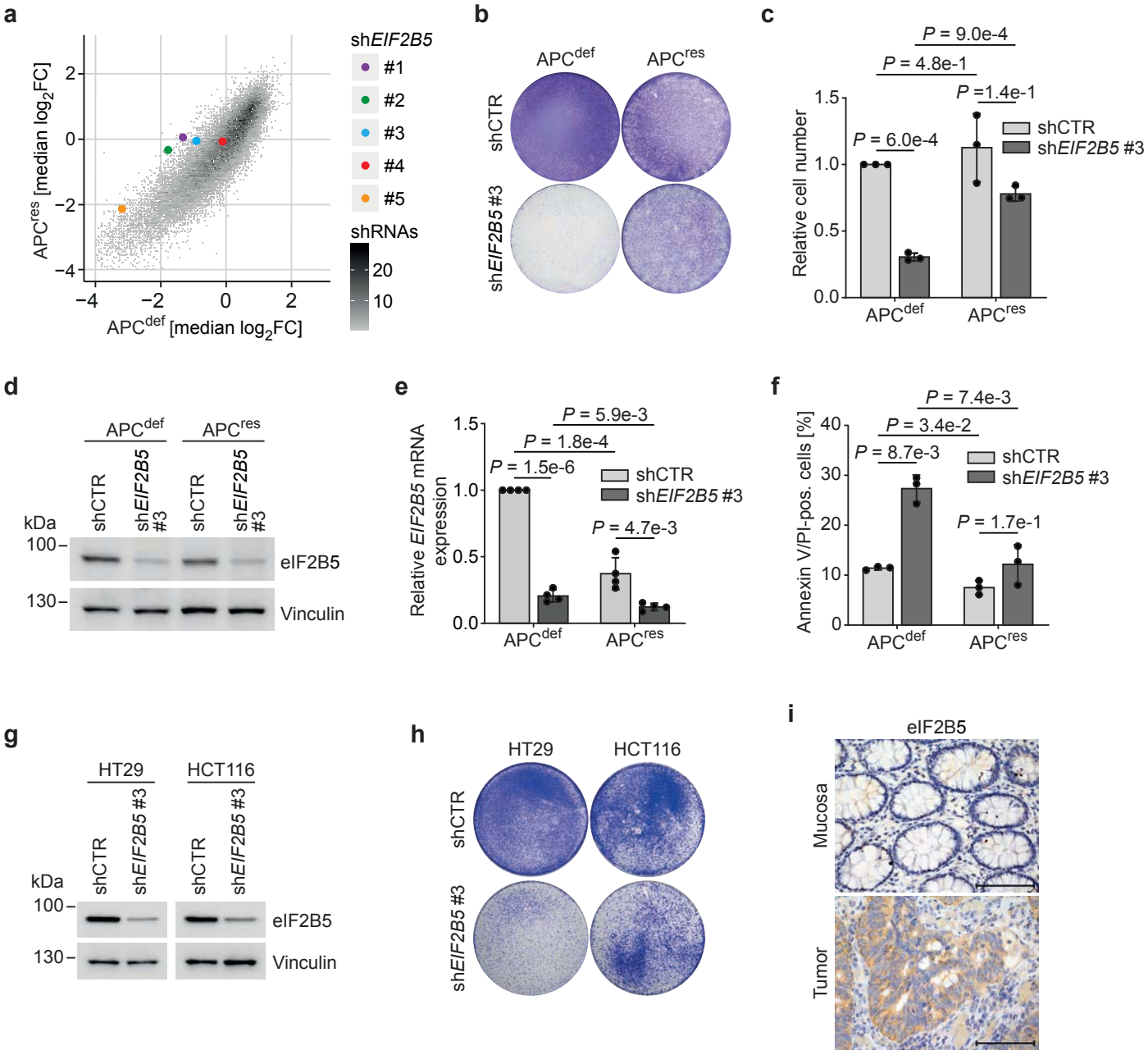
a
APC^res [median log2FC]
APC^def [median log2FC]
shEIF2B5
#1
#2
#3
#4
#5
shRNAs
20
10
b
APC^def
APC^res
shCTR
shEIF2B5 #3
c
P = 9.0e-4
P = 4.8e-1
P =1.4e-1
P = 6.0e-4
Relative cell number
shCTR
shEIF2B5 #3
APC^def
APC^res
d
APC^def
APC^res
shCTR
shEIF2B5 #3
kDa
100
130
eIF2B5
Vinculin
e
P = 5.9e-3
P = 1.8e-4
P = 1.5e-6
P = 4.7e-3
Relative EIF2B5 mRNA expression
shCTR
shEIF2B5 #3
APC^def
APC^res
f
P = 7.4e-3
P = 3.4e-2
P = 8.7e-3
P = 1.7e-1
Annexin V/PI-pos. cells [%]
shCTR
shEIF2B5 #3
APC^def
APC^res
g
HT29
HCT116
shCTR
shEIF2B5 #3
kDa
100
130
eIF2B5
Vinculin
h
HT29
HCT116
shCTR
shEIF2B5 #3
i
eIF2B5
Mucosa
Tumor

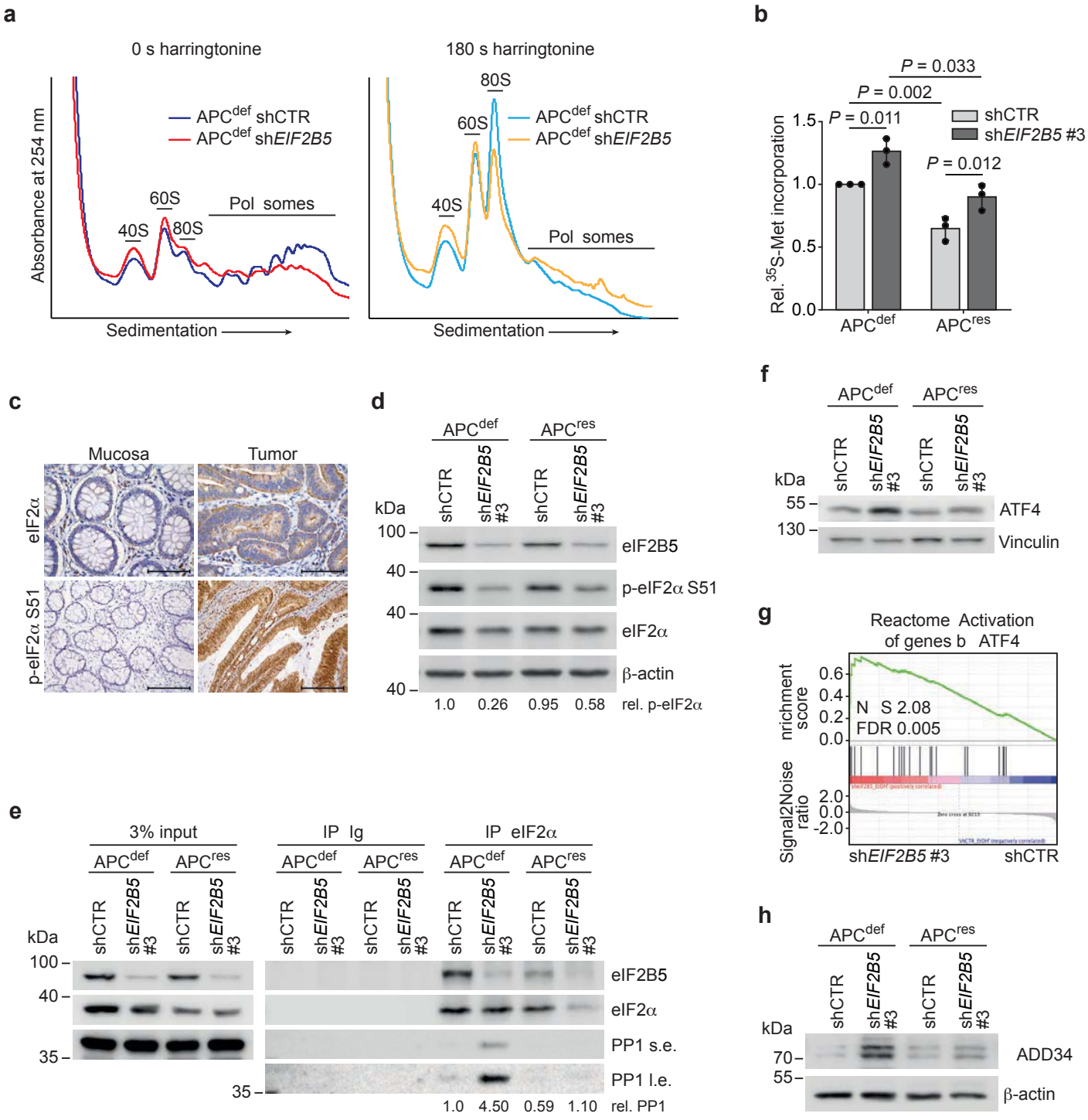
a
0 s harringtonine
180 s harringtonine
Absorbance at 254 nm
APCdef shCTR
APCdef shEIF2B5
40S
60S
80S
Pol somes
Sedimentation
b
P = 0.033
P = 0.002
P = 0.011
P = 0.012
shCTR
shEIF2B5 #3
Rel. 35S-Met incorporation
APCdef
APCres
c
Mucosa
Tumor
eIF2α
p-eIF2α S51
d
APCdef
APCres
shCTR
shEIF2B5 #3
kDa
eIF2B5
p-eIF2α S51
eIF2α
β-actin
1.0 0.26 0.95 0.58 rel. p-eIF2α
e
3% input
IP Ig
IP eIF2α
PP1 s.e.
PP1 l.e.
1.0 4.50 0.59 1.10 rel. PP1
f
ATF4
Vinculin
g
Reactome Activation of genes b ATF4
Enrichment score
N S 2.08
FDR 0.005
Signal2Noise ratio
shEIF2B5 #3
shCTR
h
ADD34
β-actin

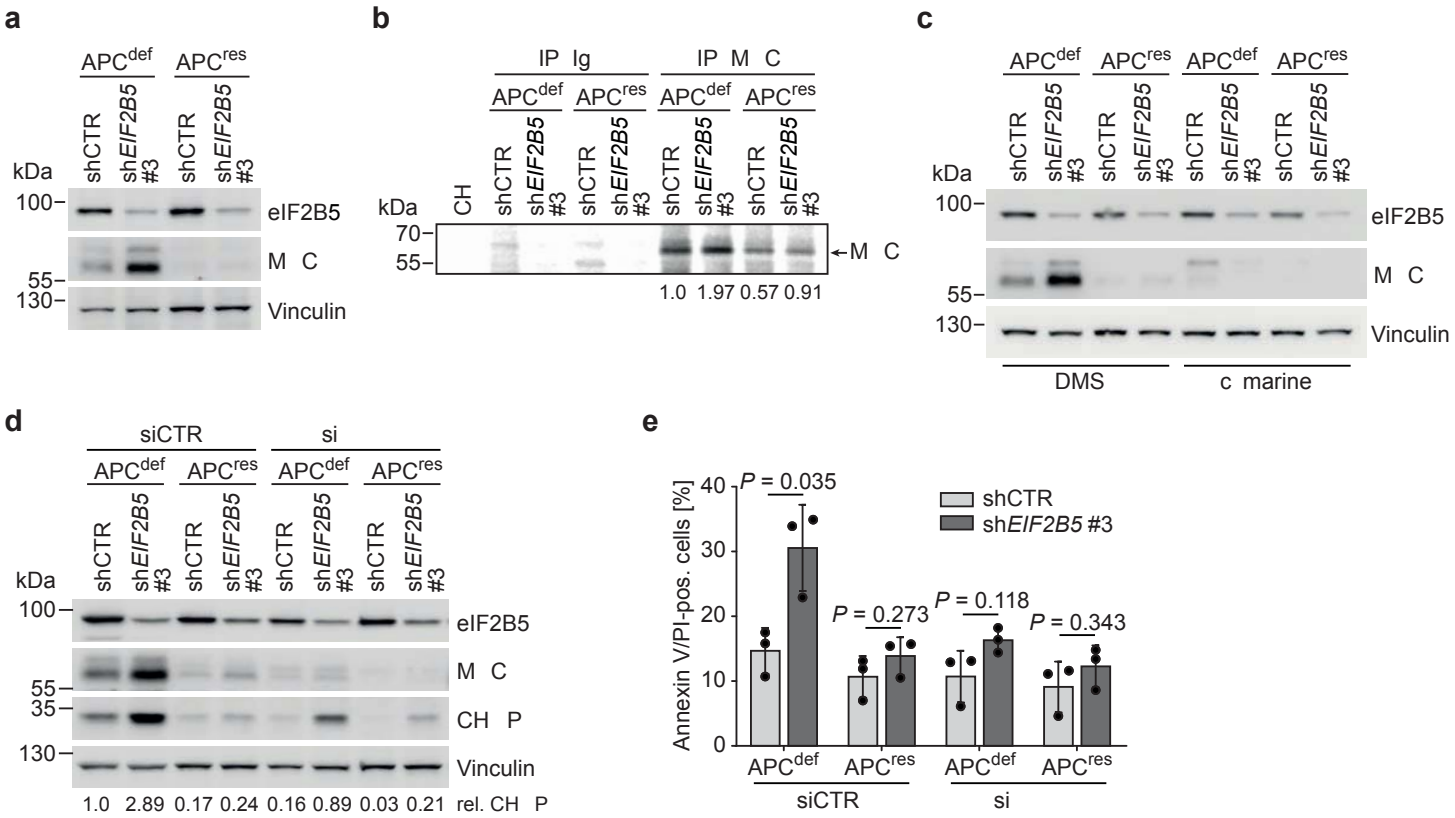
a
APC^def
APC^res
shCTR
shEIF2B5 #3
kDa
100
55
130
eIF2B5
M C
Vinculin
b
IP Ig
IP M C
CH
kDa
70
55
M C
1.0 1.97 0.57 0.91
c
DMS
c marine
d
siCTR
si
rel. CH P
1.0 2.89 0.17 0.24 0.16 0.89 0.03 0.21
CH P
e
Annexin V/PI-pos. cells [%]
P = 0.035
P = 0.273
P = 0.118
P = 0.343
shCTR
shEIF2B5 #3

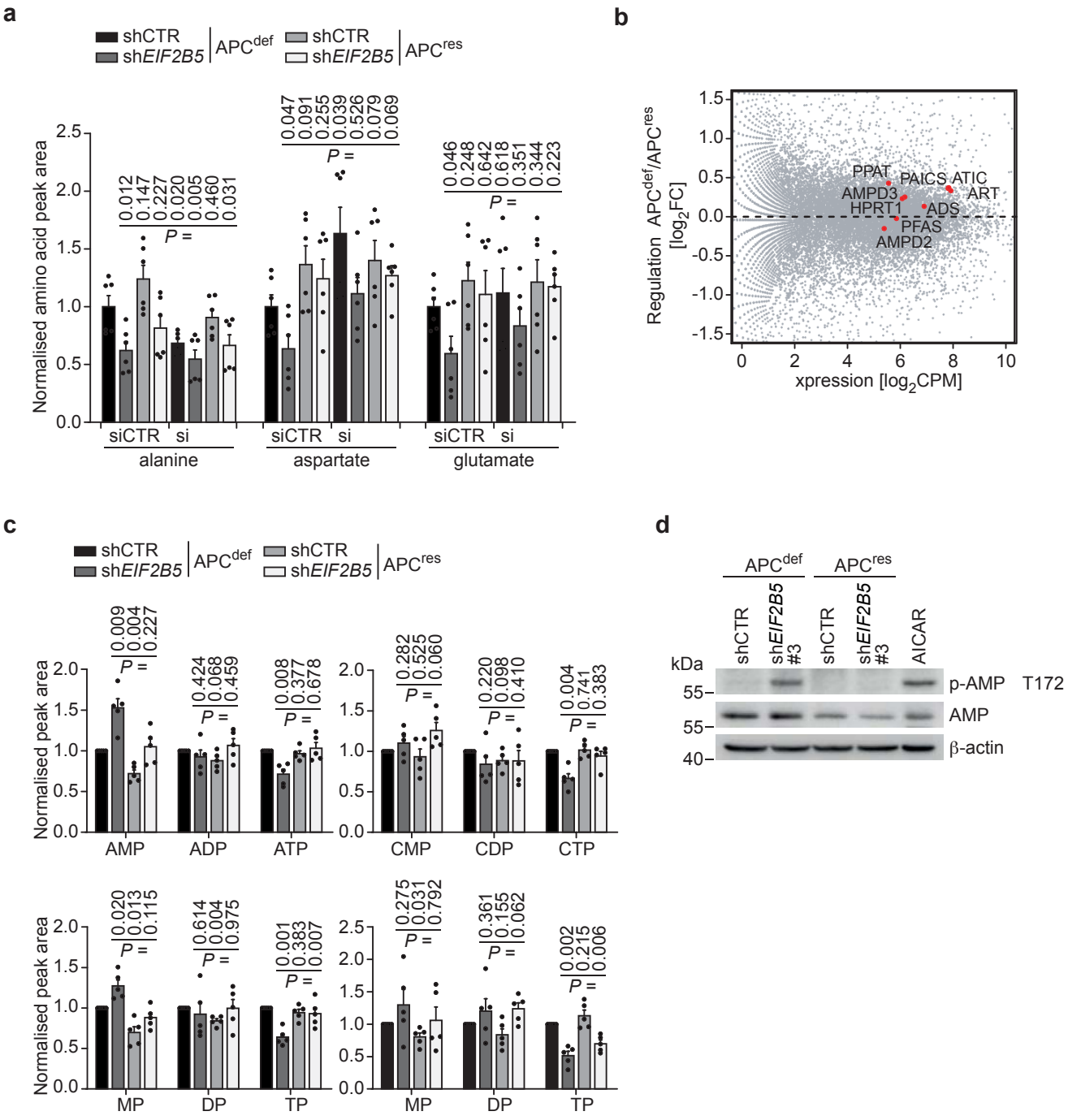
a
shCTR
shEIF2B5
APCdef
shCTR
shEIF2B5
APCres
Normalised amino acid peak area
0.012 0.147 0.227 0.020 0.005 0.460 0.031
P =
0.047 0.091 0.255 0.039 0.526 0.079 0.069
P =
0.046 0.248 0.642 0.618 0.351 0.344 0.223
P =
siCTR si
alanine
siCTR si
aspartate
siCTR si
glutamate
b
Regulation APCdef/APCres [log2FC]
xpression [log2CPM]
PPAT
PAICS
ATIC
AMPD3
ART
HPRT1
ADS
PFAS
AMPD2
c
shCTR
shEIF2B5
APCdef
shCTR
shEIF2B5
APCres
Normalised peak area
0.009 0.004 0.227
P =
0.424 0.068 0.459
P =
0.008 0.377 0.678
P =
0.282 0.525 0.060
P =
0.220 0.098 0.410
P =
0.004 0.741 0.383
P =
AMP
ADP
ATP
CMP
CDP
CTP
0.020 0.013 0.115
P =
0.614 0.004 0.975
P =
0.001 0.383 0.007
P =
0.275 0.031 0.792
P =
0.361 0.155 0.062
P =
0.002 0.215 0.006
P =
MP
DP
TP
MP
DP
TP
d
APCdef
APCres
shCTR
shEIF2B5 #3
shCTR
shEIF2B5 #3
AICAR
kDa
55
55
40
p-AMP T172
AMP
β-actin

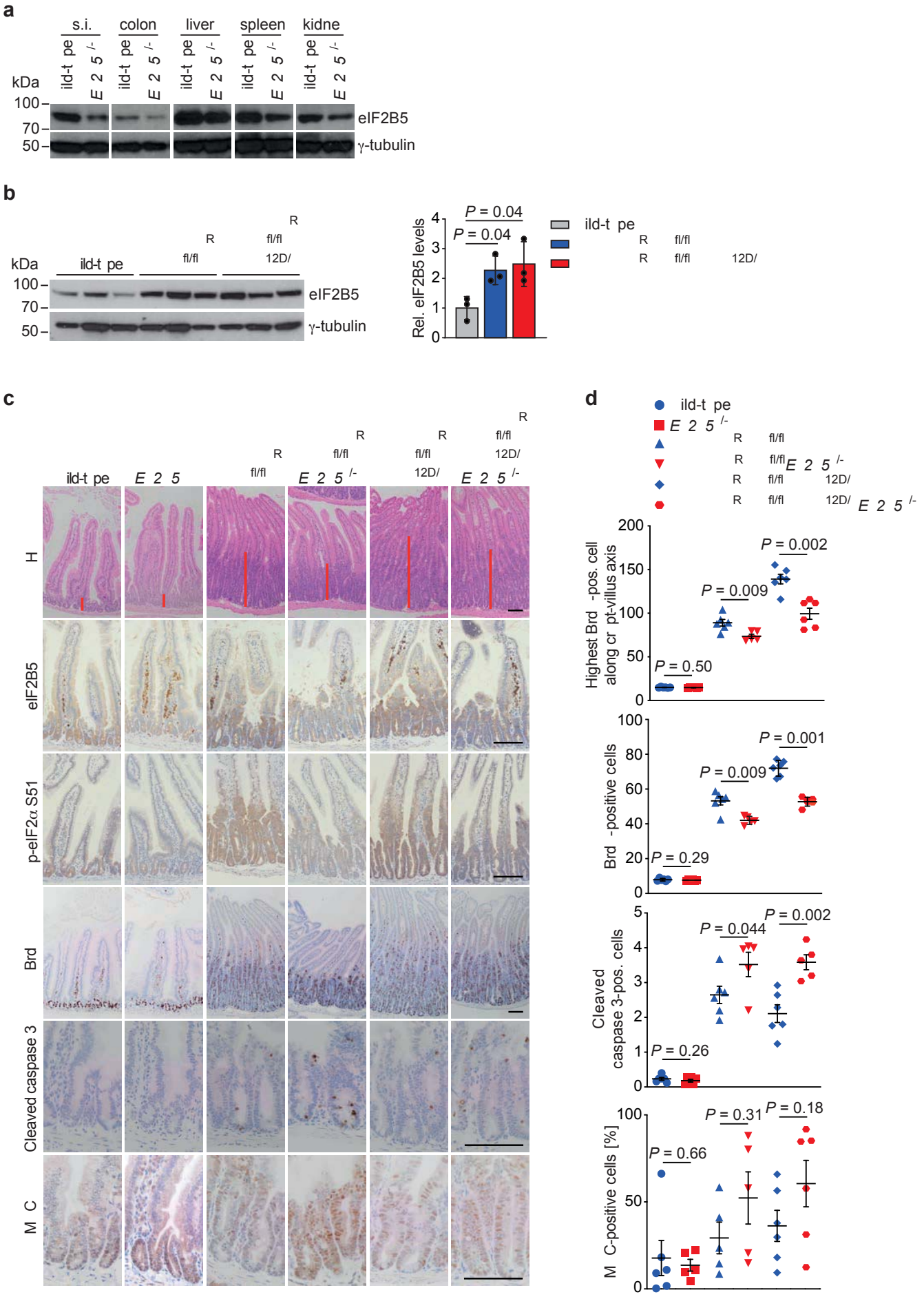
a
s.i.
colon
liver
spleen
kidne
ild-t pe
E 2 5 -/-
kDa
100
70
50
eIF2B5
γ-tubulin
b
kDa
ild-t pe
R fl/fl
R fl/fl 12D/
eIF2B5
γ-tubulin
P = 0.04
P = 0.04
Rel. eIF2B5 levels
c
ild-t pe
E 2 5
E 2 5 -/-
H
eIF2B5
p-eIF2α S51
Brd
Cleaved caspase 3
M C
d
Highest Brd -pos. cell along cr pt-villus axis
P = 0.50
P = 0.009
P = 0.002
Brd -positive cells
P = 0.29
P = 0.009
P = 0.001
Cleaved caspase 3-pos. cells
P = 0.26
P = 0.044
P = 0.002
M C-positive cells [%]
P = 0.66
P = 0.31
P = 0.18

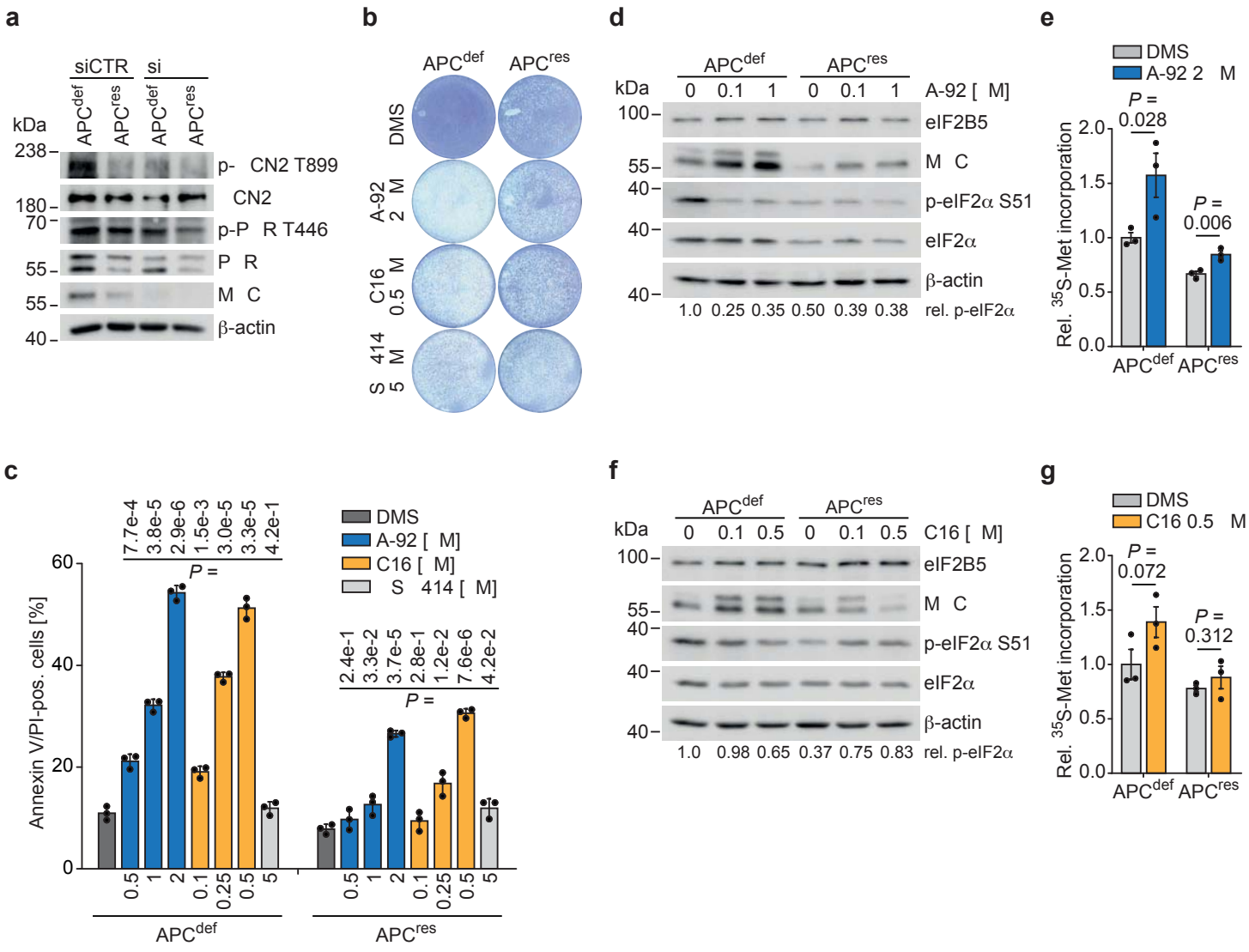
a
siCTR
si
APCdef
APCres
APCdef
APCres
kDa
238
p- CN2 T899
180
CN2
70
p-P R T446
55
P R
55
M C
40
β-actin
b
APCdef
APCres
DMS
A-92 2 M
C16 0.5 M
S 414 5 M
d
APCdef
APCres
kDa
0 0.1 1 0 0.1 1
A-92 [M]
100
eIF2B5
55
M C
40
p-eIF2α S51
40
eIF2α
40
β-actin
1.0 0.25 0.35 0.50 0.39 0.38
rel. p-eIF2α
e
DMS
A-92 2 M
P = 0.028
P = 0.006
Rel. 35S-Met incorporation
2.0
1.5
1.0
0.5
0.0
APCdef
APCres
c
7.7e-4 3.8e-5 2.9e-6 1.5e-3 3.0e-5 3.3e-5 4.2e-1
P =
DMS
A-92 [M]
C16 [M]
S 414 [M]
2.4e-1 3.3e-2 3.7e-5 2.8e-1 1.2e-2 7.6e-6 4.2e-2
P =
Annexin V/PI-pos. cells [%]
60
40
20
0
0.5 1 2 0.1 0.25 0.5 5
APCdef
APCres
f
APCdef
APCres
kDa
0 0.1 0.5 0 0.1 0.5
C16 [M]
100
eIF2B5
55
M C
40
p-eIF2α S51
40
eIF2α
40
β-actin
1.0 0.98 0.65 0.37 0.75 0.83
rel. p-eIF2α
g
DMS
C16 0.5 M
P = 0.072
P = 0.312
Rel. 35S-Met incorporation
2.0
1.5
1.0
0.5
0.0
APCdef
APCres

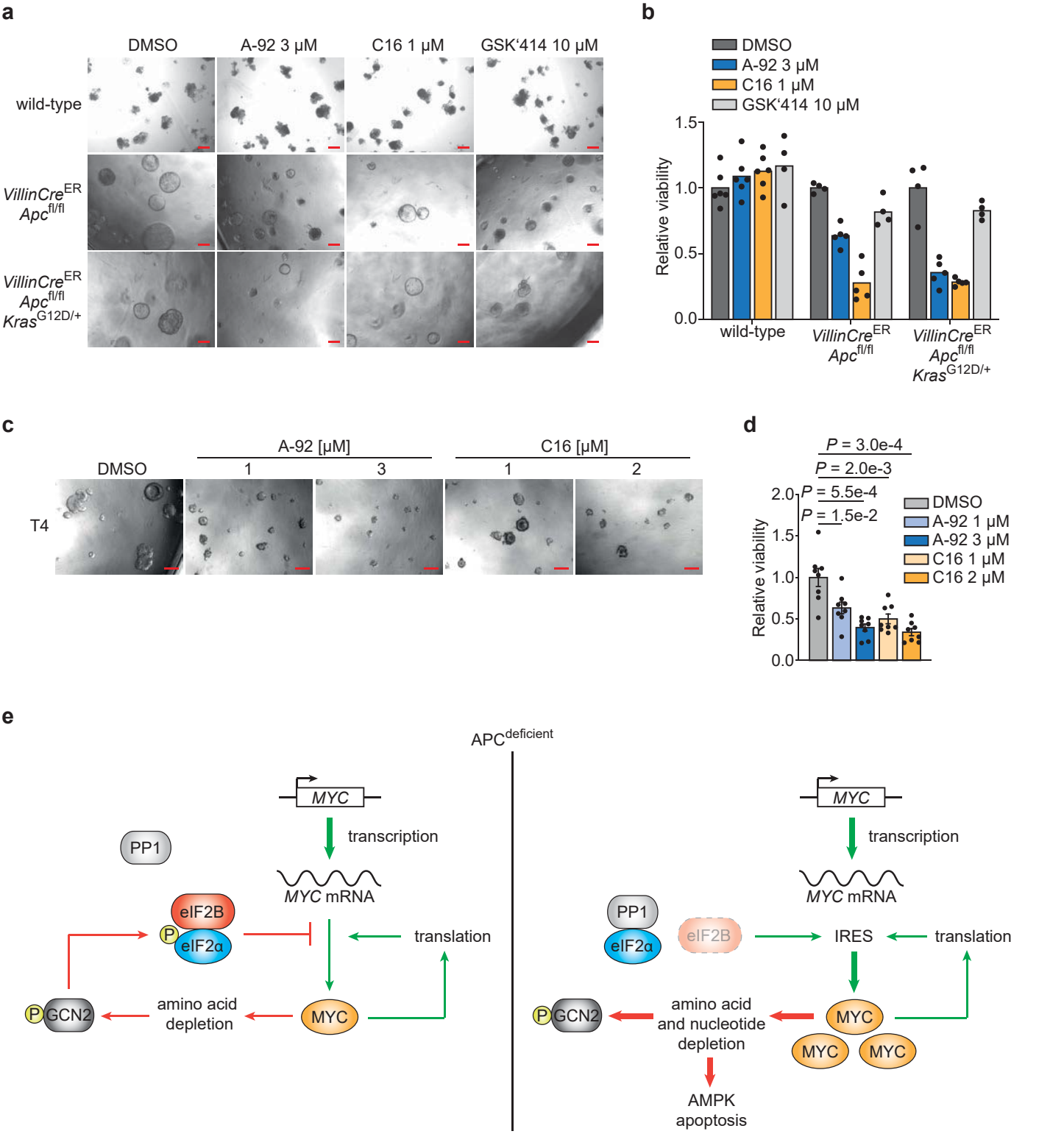
a
DMSO
A-92 3 µM
C16 1 µM
GSK'414 10 µM
wild-type
VillinCre^ER Apc^fl/fl
VillinCre^ER Apc^fl/fl Kras^G12D/+
b
DMSO
A-92 3 µM
C16 1 µM
GSK'414 10 µM
Relative viability
1.5
1.0
0.5
0.0
wild-type
VillinCre^ER Apc^fl/fl
VillinCre^ER Apc^fl/fl Kras^G12D/+
c
A-92 [µM]
C16 [µM]
DMSO
1
3
1
2
T4
d
P = 3.0e-4
P = 2.0e-3
P = 5.5e-4
P = 1.5e-2
Relative viability
2.0
1.5
1.0
0.5
0.0
DMSO
A-92 1 µM
A-92 3 µM
C16 1 µM
C16 2 µM
e
APC^deficient
MYC
transcription
MYC mRNA
PP1
eIF2B
P
eIF2α
translation
P GCN2
amino acid depletion
MYC
MYC
transcription
MYC mRNA
PP1
eIF2α
eIF2B
IRES
translation
P GCN2
amino acid and nucleotide depletion
MYC
MYC
MYC
AMPK apoptosis

Extended Data 1

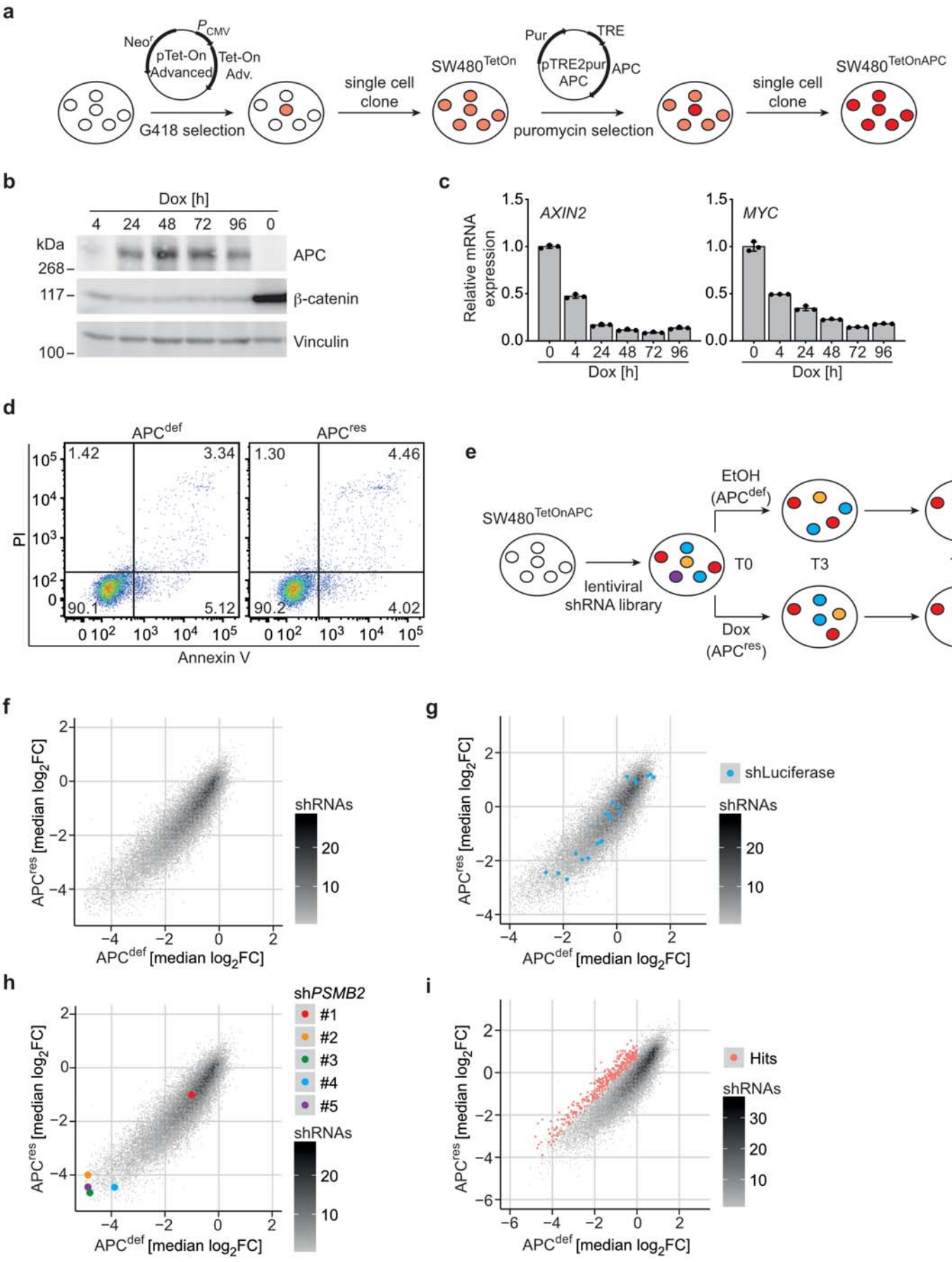

Extended Data 2

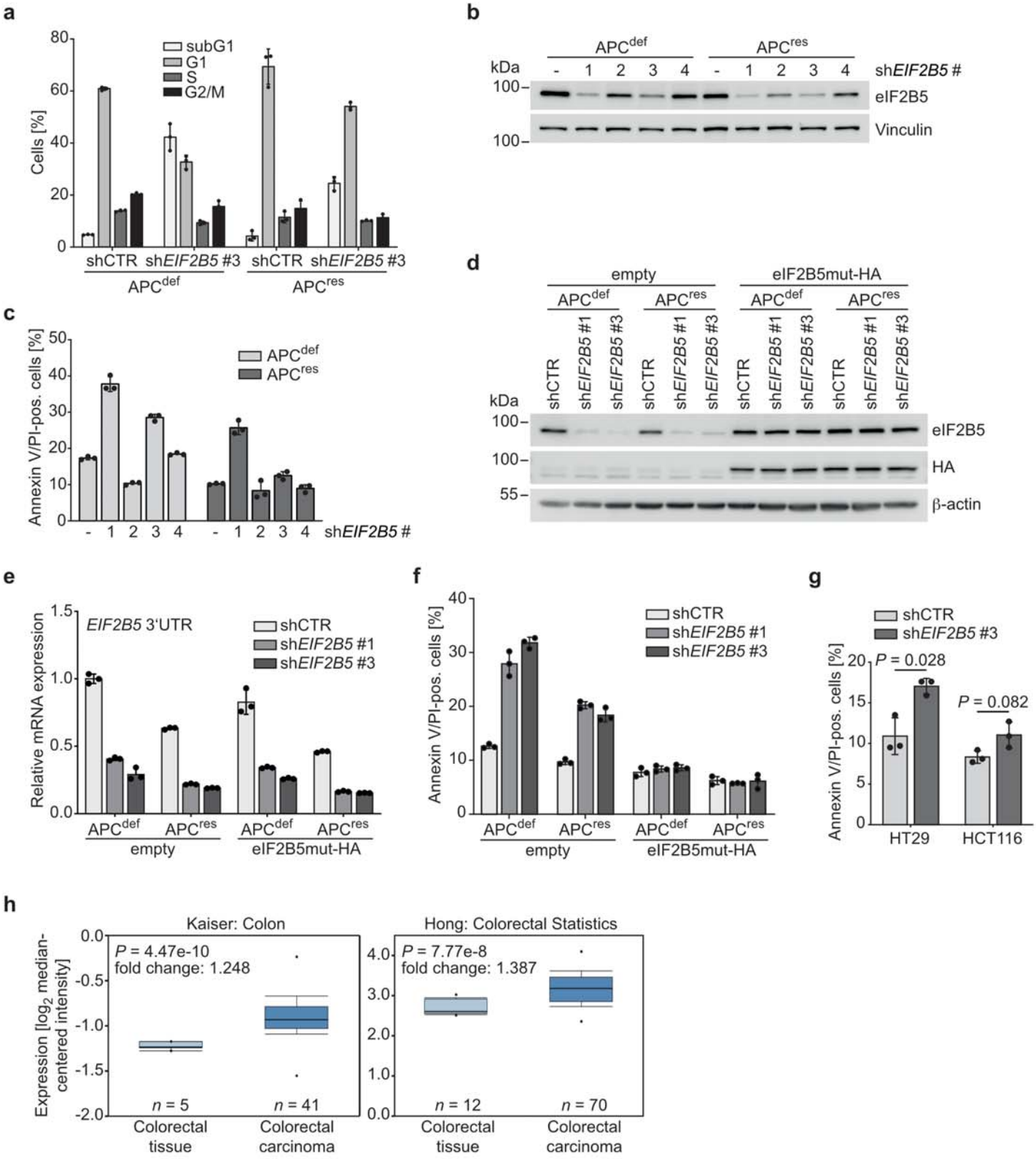

Extended Data 3

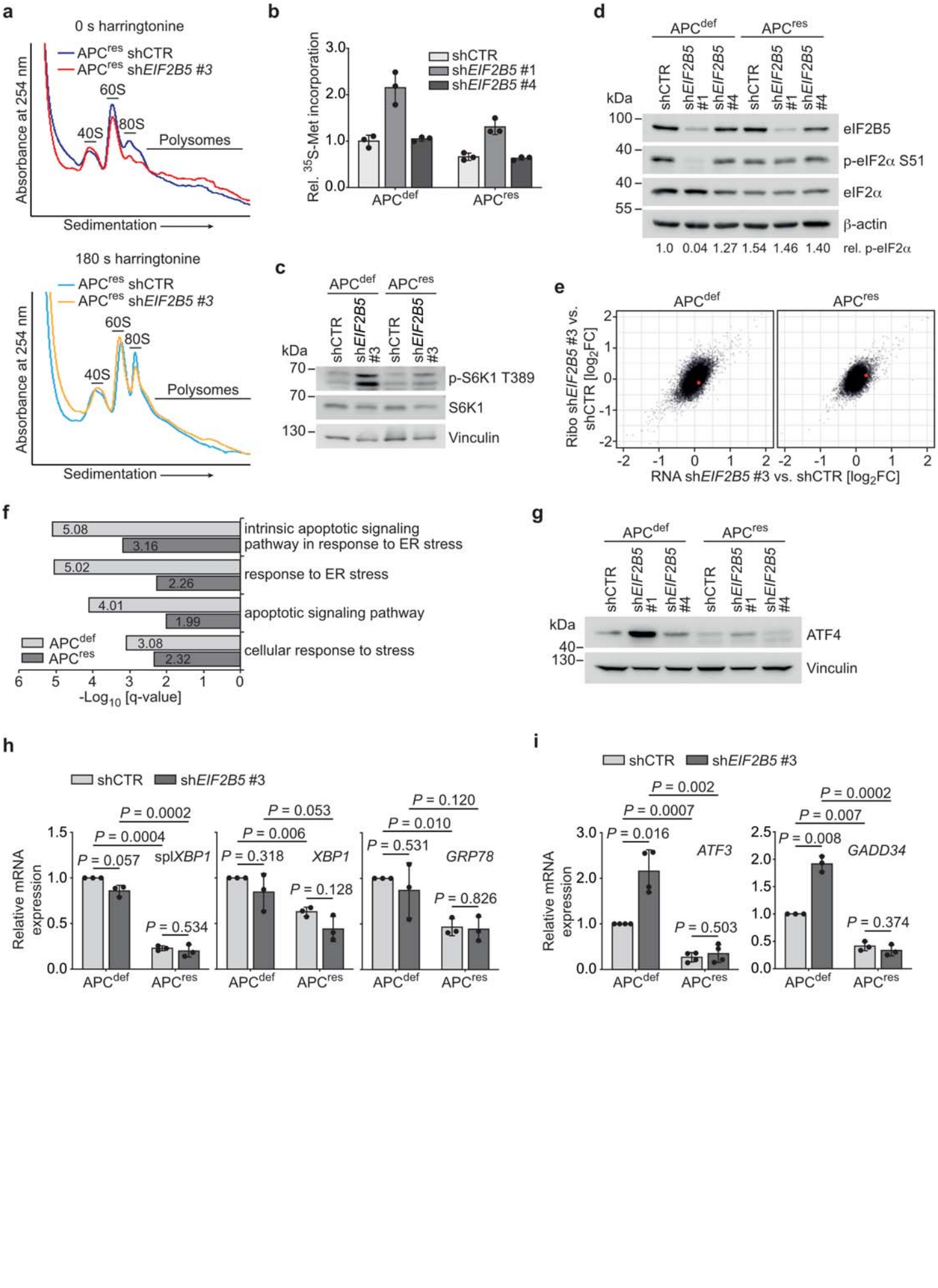

Extended Data 4

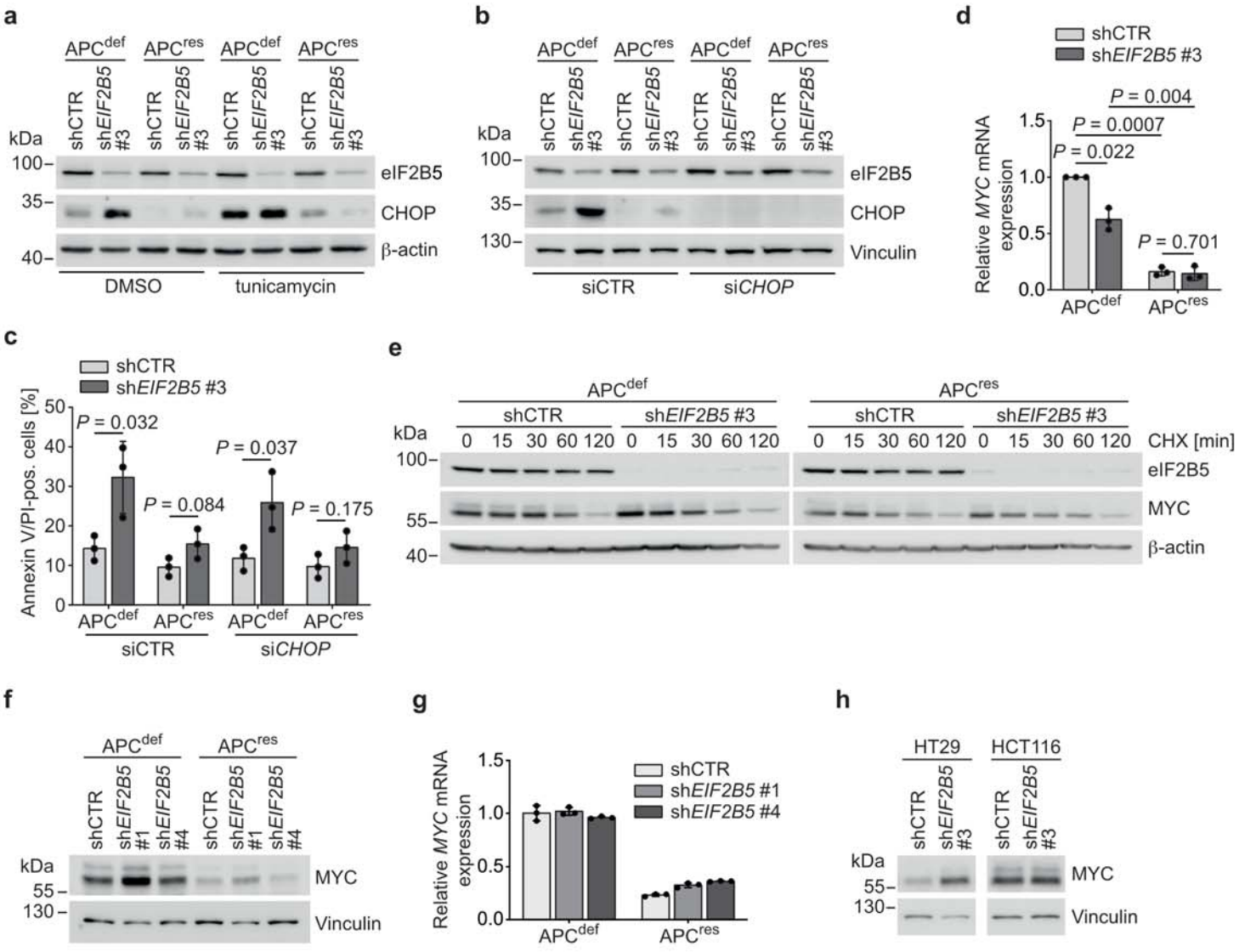

Extended Data 5

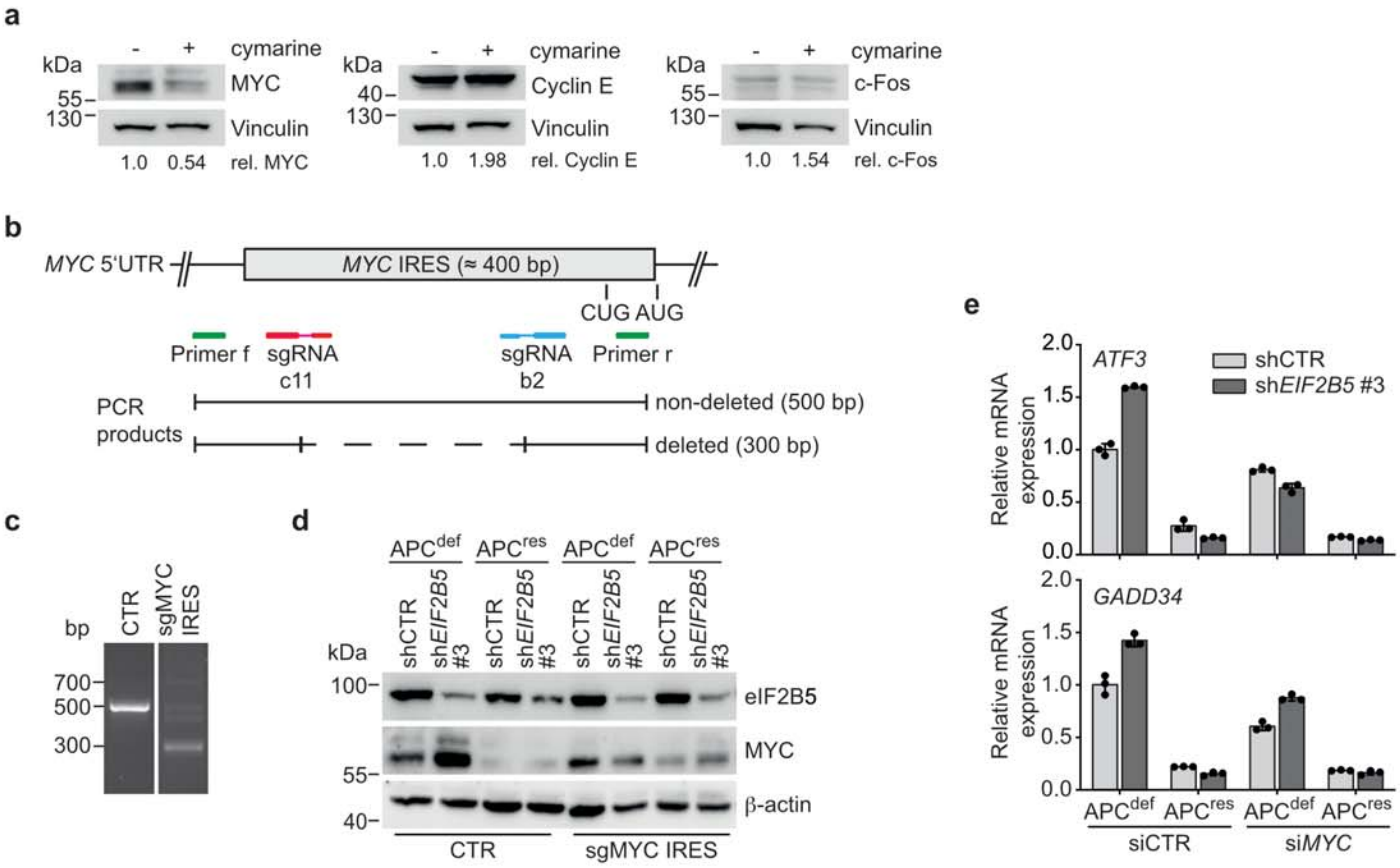

Extended Data 6

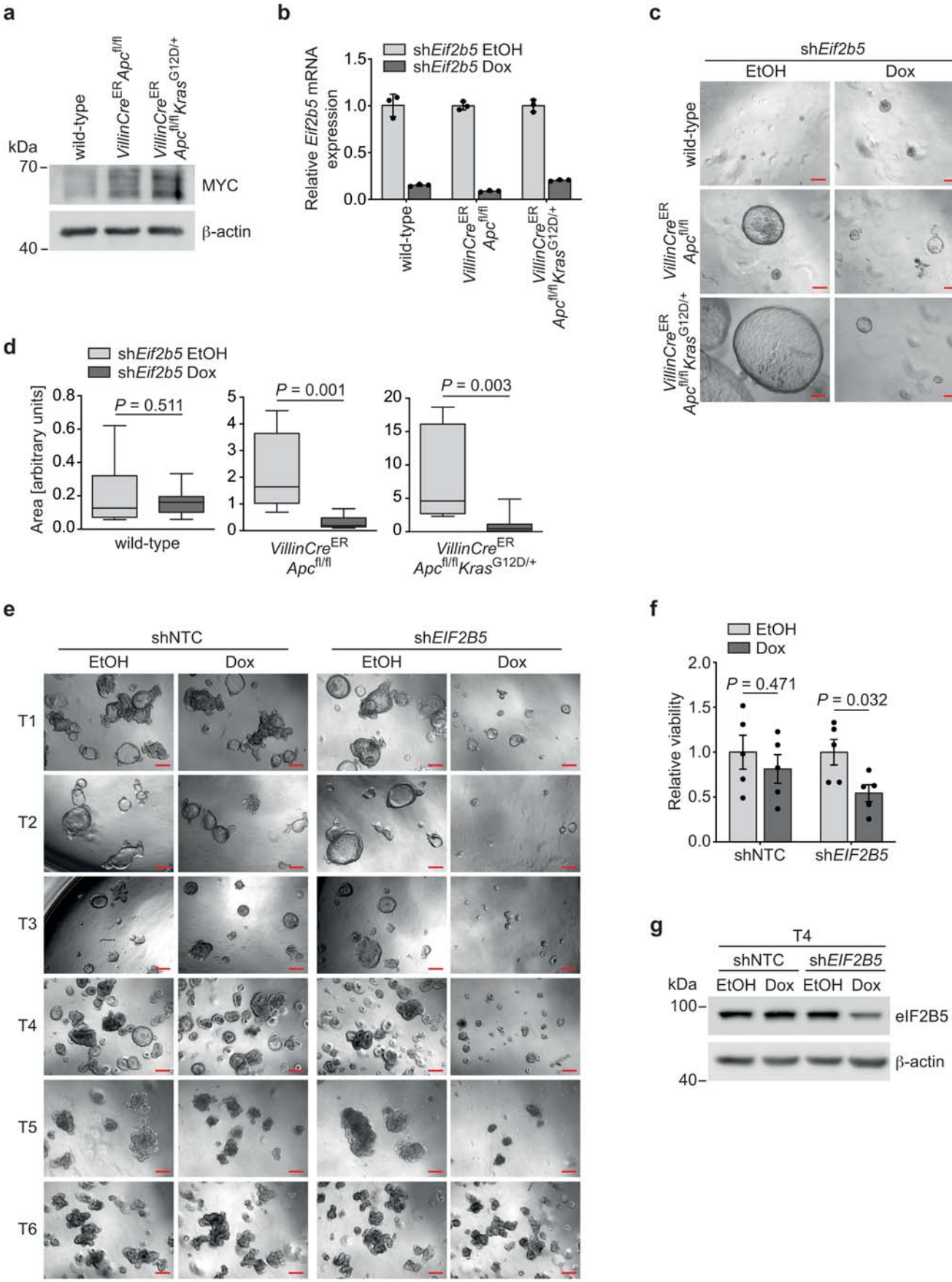

Extended Data 7

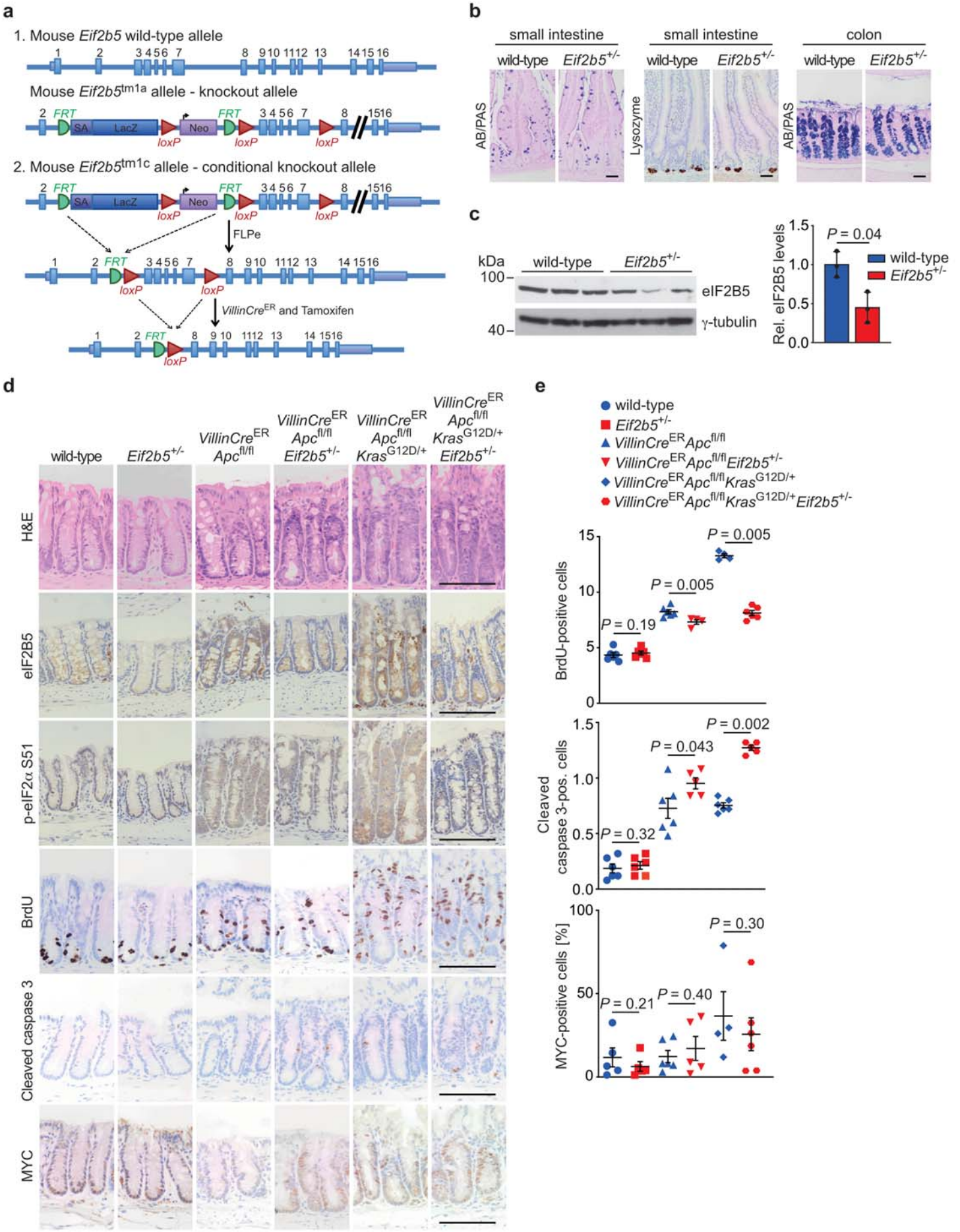

Extended Data 8

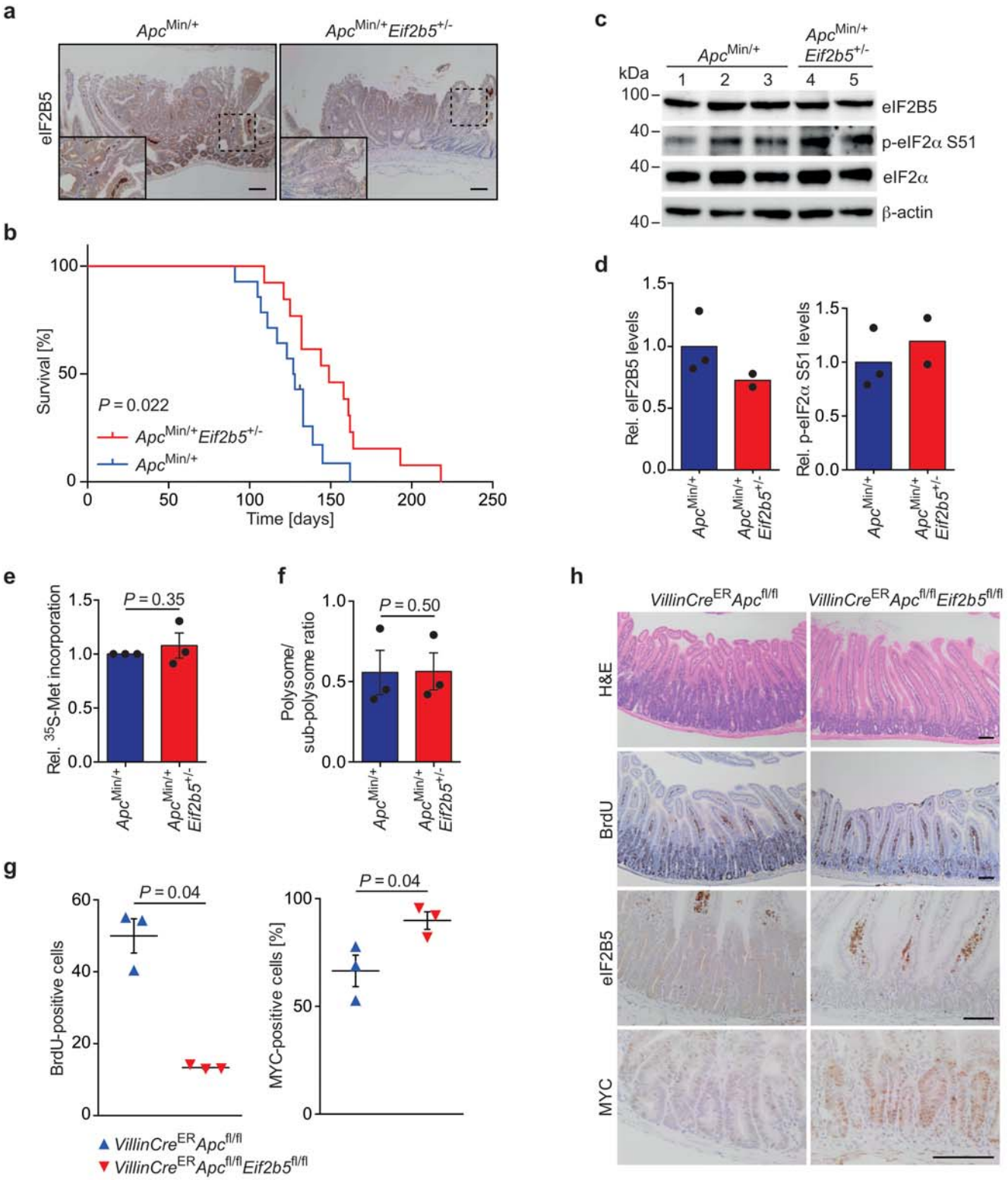

Extended Data 9

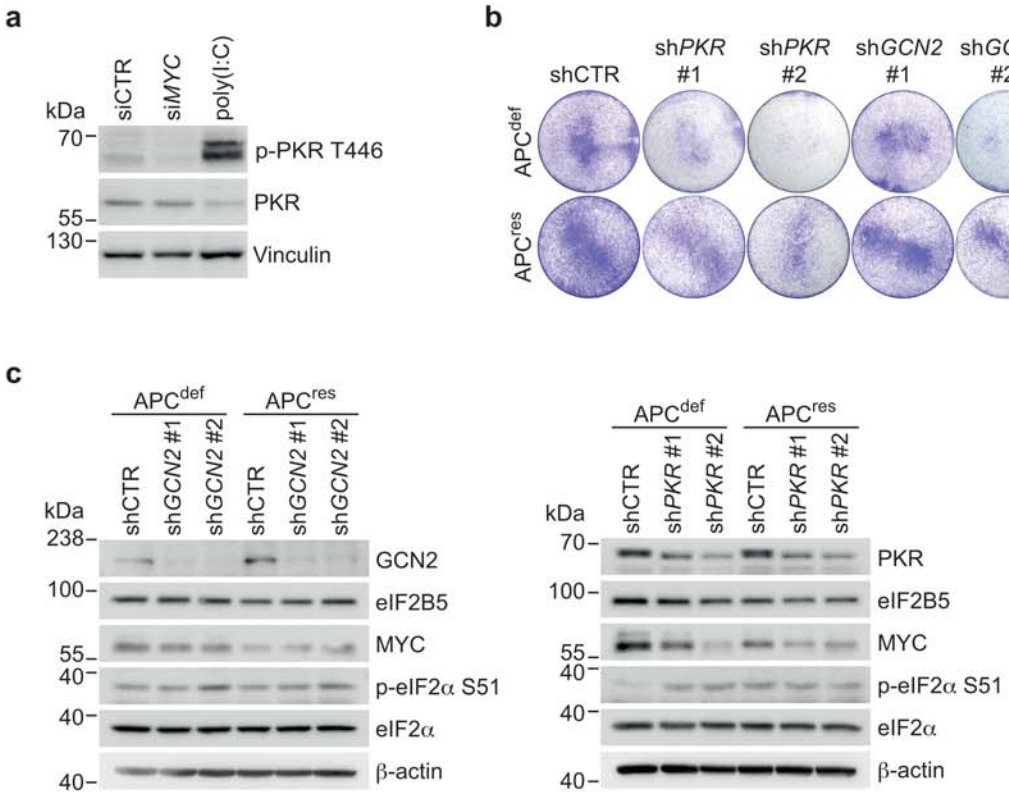

Extended Data 10